Nonlinear Dyn (2021) 103:809–832
https://doi.org/10.1007/s11071-020-06126-z

ORIGINAL PAPER

# Coordinated control strategy for mode transition of DM-PHEV based on MLD

**Cong Liang · Xing Xu · Feng Wang · Zhiguang Zhou**

Received: 3 July 2020 / Accepted: 1 December 2020 / Published online: 5 January 2021


**Abstract** In this paper, a hybrid variable cost function model predictive control strategy (HC-MPC) is developed for the mode transition process of a novel motor compound power-split plug-in hybrid electric vehicle (DM-PHEV). Based on the layout of DM-PHEV, the mode transition process from electric driving mode to hybrid driving mode is divided into 5 stages. Considering the hybrid characteristics of mode transition process, the dynamic models under different stages are transmitted into an equivalent mixed-logical dynamical hybrid model. MPC based on hybrid model (H-MPC) is applied as the coordinated controller. Moreover, considering that fixed cost functions for the finite time horizon are not reasonable if stage transition happened during the prediction horizon, so variable cost functions changing with predictable stages is useful for improving the control effect of MPC. H-MPC considering variable cost functions (HC-MPC) is proposed as the coordinate controller in this paper. Simulation and hardware-in-the-loop test show that HC-MPC can efficiently improve the PHEV drivability.

**Keywords** PHEV · Mode transition · Hybrid systems · Variable cost functions · MPC · LQR

C. Liang · X. Xu (✉)· F. Wang
Automotive Engineering Research Institute, Jiangsu University, Zhenjiang 212013, Jiangsu, People's Republic of China
e-mail: xuxing@mail.ujs.edu.cn

C. Liang · X. Xu · F. Wang
School of Automotive and Traffic Engineering, Jiangsu University, Zhenjiang, People's Republic of China

Z. Zhou
New Energy Development Department Powertrain Technology Center, Chery Automobile Company, Wuhu, People's Republic of China

## List of symbols

| | |
|---|---|
| $T_{\text{en\_cmd}}$ | Engine torque command |
| $\tau_{\text{en}}$ | Time constant of engine |
| $T_{\text{en\_fric}}$ | Resistance torque of engine |
| $n_{\text{m1}}$, $n_{\text{m2}}$ | Speed of motor 1, 2 |
| $T_{\text{m1\_cmd}}$, $T_{\text{m2\_cmd}}$ | Torque command of motor 1, 2 |
| $x_{\text{p0}}$ | Initial displacement compressed on return spring |
| $x_{\text{p}}$ | Displacement of clutch piston away the initial position |
| $F_{\text{cl}}$ | Reaction force of clutch friction plate on piston |
| $Q_{\text{c}}$ | Average flow of clutch |
| $V_0$ | Volume of clutch oil chamber |
| $\rho$ | Hydraulic oil density |
| $P_s$ | Oil pressure provided by the tank |
| $A_h$ | Area of valve supporting port |
| $\bar{Q}_{\text{in}}$ | Average flow of supplying port |
| $P_0$ | Oil pressure of gearbox |
| $J_{\text{m1}}$ | Equivalent inertia moment of motor 1 and planetary gears |
| $J_r$ | Inertia moment of clutch driving shaft speed |

| | |
|---|---|
| $\omega_l$ | Clutch driven shaft speed |
| $J_\mathrm{p}$ | Inertia moment of planetary mechanism |
| TDS | Equivalent elastic shaft of the tire and half shaft |
| $k_\mathrm{TDS}$ | Equivalent torsional stiffness of TDS |
| $C_\mathrm{TDS}$ | Equivalent damping coefficient of TDS |
| $i_0$ | Final drive ratio |
| $C_\mathrm{d}$ | Air drag coefficient |
| $\theta$ | Angular displacement |
| $m_\mathrm{veh}$ | Vehicle mass |
| $\eta_\mathrm{t}$ | Efficiency of transmission system |
| $\alpha$ | Road slope |
| $n_\mathrm{thresh}$ | Speed limit of engine drag torque change |
| $z_i$ | Continuous auxiliary variables |
| $A_\mathrm{fric}$ | Engine resistance torque coefficient |
| $W$ | Clutch slipping energy |
| $Q$, $R$ | Weight matrix |
| $T_\mathrm{en}$ | Output torque of engine |
| $n_\mathrm{en}$ | Engine speed |
| $T_\mathrm{m1}$, $T_\mathrm{m2}$ | Output torque of motor 1, 2 |
| $\tau_\mathrm{m1}$, $\tau_\mathrm{m2}$ | Time constant of motor 1, 2 |
| $k_p$ | Stiffness of the clutch return spring |
| $s_\mathrm{max}$ | Maximum displacement away the initial position |
| $F_\mathrm{p}$ | Static pressure on clutch piston |
| $A_\mathrm{C2}$ | Clutch piston area |
| $x_\mathrm{max}$ | Maximum clutch piston displacement |
| $\beta$ | Effective volume elastic modulus of hydraulic fluid |
| $P_\mathrm{c}$ | Control pressure of clutch |
| $C_h$ | Valve flow coefficient |
| $\tau$ | Duty cycle of PWM |
| $\tilde{Q}_\mathrm{out}$ | Average flow of recycle port |
| $J_\mathrm{en}$ | Inertia moment of engine |
| $J_\mathrm{m2}$ | Equivalent inertia moment of motor 2 and clutch disc |
| $J_\mathrm{veh}$ | Vehicle equivalent inertia |
| $\omega_r$ | Clutch driving shaft speed |
| TH | Torsional damper spring |
| $k_\mathrm{TH}$ | Equivalent torsional stiffness of TH |
| $C_\mathrm{TH}$ | Equivalent damping coefficient of TH |
| $i_2$ | Gear ratio of motor 2 |
| $T_f$ | Equivalent running resistance torque of vehicle |
| $A$ | Effective frontal area |
| $v$ | Vehicle speed |
| $f$ | Roll resistance coefficient |
| $R$ | Radius of tire |
| $\delta_i$ | Introducing binary auxiliary variable |
| $T_\mathrm{ega}$, $n_\mathrm{ega}$ | Predefined positive scalar |
| $j$ | Vehicle jerk |
| $J_i$ | Cost function |
| $\varepsilon$ | Auxiliary variables in cost functions |
| $x_e$ | State variable reference value |

## 1 Introduction

The development of automotive industry has always been closely connected with energy. With the increasing demands on reducing the emission of greenhouse gases, the transformation of automotive energy power source is inevitable. The development of electric vehicles (EV) is limited by the capacity of battery, so hybrid electric vehicles (HEV) have become one of the research hotspots because of their energy-saving and low-emission characteristics while meeting the mileage requirements [1–4]. Compared with traditional HEV, the compound power-split PHEV integrates the advantages of series and parallel hybrid vehicles. However, its structure is much more complicated than traditional HEV, which makes it much more difficult to control [5].

With more actuators and more freedom, PHEVs need to decide the power distribution between each power source, energy management control strategy (EMC) is proposed to optimize the working mode and amount of power that each power source provides to minimize the fuel consumption while meet the driver demand according to the specific driving cycles [6–8]. If the road conditions and the states of the vehicle change, EMC may give the instruction of mode transition. Wang [9] proposed a novel EMC which choose the comprehensive dynamic efficiency of whole powertrain as a single optimization objective to improve the fuel economy. Xu [10] proposed a novel EMC which considers cooling power demand and effect of temperature on fuel economy. However, EMC only gives mode

transition instruction but does not consider the dynamic characteristics of actuators such as engine start process during the mode transition process. The vehicle jerk during mode transition process effects the drivability of PHEVs, so a coordinated controller which works to improve the driving comfort of PHEVs during mode transition process is necessary.

The architecture of PHEV decides the key goal of coordinated controller. For PHEVs without clutch which located between the engine and motor, the key problem is the engine ripple torque (ERT) that is generated at low engine speeds. Because TDS can only isolate high-frequency engine torque fluctuations when engine is operating at normal speed. Large oscillations may be caused by ERT during mode transition process. In response to this problem, Wang et al. proposed an active damping torque calculation system [11] to suppress driveline speed oscillations based on the estimations of carrier torque which consider the effects of ERT. Another key problem of this architecture is that the engine response speed is significantly slower than motors when engine is started, so the coordination of torque changing rate of power sources is considered in many studies. Zeng [12] designed a predictive-model-based coordinated control strategy which considered the different response speed of power sources and MPC is used to predict the degree of shock. Liu [13] proposed a sliding mode controller which suppressed the engine torque fluctuation through electric motor for mode transition process. However, for PHEVs with engine clutch that located between the engine and motor [14], the strong nonlinear dynamic characteristics introduced by clutch and its hydraulic system must be considered. As engine can be started by clutch engagement, thus the mode transition performance mainly depends on the control of clutch engagement and the coordination of motor torque and clutch torque. Many researches have been conducted. Yang [15] adopted two approaches to acquire the expected clutch position trajectory by compromising the vehicle jerk and clutch slipping energy. What's more, considering the uncertainties exists in the engine resistance torque for the clutch engagement of mode transition process, Yang [16] proposed a robust H-infinity controller. Wang [17] presented a novel multi-objective function for the establishment of clutch oil pressure process which considers the vehicle jerk and fatigue life of planetary hybrid power-split system. However, these studies only included the clutch slipping process, and the other stages of mode transition process are not considered. Besides, the coordination between motors and clutch are also neglected. For the DM-PHEV architecture investigated in this research, auxiliary motor and engine are on the driven disc side of clutch, so engine can be started by auxiliary motor before clutch engagement, which can avoid engine ripple torque at low engine speed. Therefore, coordinated control of engine, two motors and clutch is needed. Song et al. proposed that the mode transition process can be divided into three stages: engine cranking phase, speed synchronization phase and torque switching phase [18]. Different control strategies were designed for every phase to reduce torque fluctuation. Gao et al. considered the friction-induced discontinuity of clutch torque and ICE on/off and proposed a sliding mode control strategy to improve riding comfort [19]. The switching process was also divided into three phases, and three sliding mode controllers were designed to coordinate the torque of power sources. However, the stability of switching between several controllers are not considered in these studies, and the performance of mode transition during controller switching is also difficult to guarantee.

Few studies considered that the coordinated control of PHEV in mode transition process can be characterized as a hybrid control problems as the process can be divided into several stages. A hybrid system is a unified dynamic system formed by the interaction of continuous and discrete variable dynamic systems [20]. For the continuous variable dynamic system (CVDS), several state-space equations are needed to describe different stages of mode transition. Furthermore, CVDS model requires the switching of controllers for each stage, which is difficult to obtaining more optimized results and even reducing system stability. While a hybrid system is a unified dynamic system formed by the interaction of continuous and discrete variable dynamic systems, so one hybrid system controller can perfectly meet the requirements. MLD is kind of hybrid system [21,22] which allows to define system models in the discrete-time domain, and the nonlinear dynamics of system can be transformed into affine dynamics. Mode switching is a short-term process that requires high stability, thus, MLD is a better choice for the modelling of mode transition process. MLD has been applied in some researches. Kou et al. [23] designed the energy management strategy of hybrid electric bus based on MLD, and then solved the problem by turning it into a mixed integer linear programming (MILP). Simulation

results show that the H-MPC controller improved fuel economy and reduced emissions. Sun [24] proposed a hybrid model predictive control (HMPC) strategy to regulate the longitudinal velocity considering the nonlinear tire dynamics. The tire longitudinal dynamics is accurately modelled by piecewise affine identification and transformed into MLD model, then MPC strategy is applied as the speed tracking controller. Although MLD has been applied to PHEVs, few papers considered the hybrid characteristics of mode transition process and use MLD to model the mode transition process. And the MPC controller proposed before only consider the state of system changing with mode, changes of cost functions during the prediction process have not been considered.

The mode transition process from electric driving mode (EM) to hybrid driving mode (HM) involves engine start and clutch engagement process, which is the most complicated mode transition process from EM to HM for PHEVs. During this process, inconsistent characteristics of engine and motors, nonlinear dynamic characteristics of clutch can directly cause jerk and vibration to power-train [25]. Based on the aforementioned analysis, this paper firstly proposed a HC-MPC controller for the mode transition process from EM to HM of DM-PHEV, which can avoid the switching between multiple controllers to insure the stability of mode transition process. The original contribution of this paper is summarized as follows. Firstly, the mode transition process from EM to HM is analysed and divided into five stages according to the dynamic characteristics. After establishing the dynamic model, to avoid the controller switching at different stages, a unified state-space equation of DM-PHEV is modelled using MLD for the first time. Furthermore, different cost function of each stage is considered, in the clutch slipping stage, both the vehicle jerk and clutch slipping energy loss are considered, which is hard for MPC to find a global optimal solution, so LQR controller is combined with hybrid MPC to help improve the control effect. Moreover, this paper firstly gives a solution of variable cost functions with the predicted stages during prediction domain of MPC, which will be helpful to acquire better effects of prediction. Finally, a HC-MPC control is utilized as the coordinated controller.

This paper is organized as follows. Firstly, a novel compound power-split PHEV model is built in Sect. 2, which is used to verify the control strategy. In Sect. 2.1, the state-space equation during mode transition process is given and the process is divided into 5 stages, which can be unified using MLD model, the MLD model is also given in Sect. 2.1. Section 3 analyses the object of coordinate control and designs the H-MPC controller and HC-MPC controller. Simulation and HiL results are given in Sect. 4. In the end, the conclusion is drawn in Sect. 5.

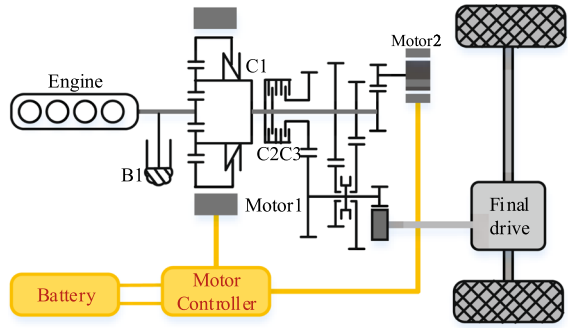


**Fig. 1** Schematic diagram of the DM-PHEV

## 2 PHEV power-train modelling

The configuration of DM-PHEV is shown in Fig. 1. The hybrid transmission is made up of one engine, two motors and one compound power-split device. The power-split device consists of one ring gear, one sun gear, four planet gears and one planet carrier. The sun gear is connected to the engine crankshaft through a torsional damper system (TDS), and can be locked by the brake device (B1). Motor 1 serves as an auxiliary power, which can be coupled to the engine through the ring gear, it can also be used as a starting motor. The power coupling mechanism drives the PHEV together with the motor 2 through the dual-clutch gearbox. Dual motors can improve both the dynamic performance and the fuel economy of DM-PHEV. Through the control of three clutches and one brake, the vehicle can work in different modes.

A model of DM-PHEV is developed to characterize the dynamic behaviour during mode transition process. As show in Fig. 1, this model contains 4 modules: engine, motor, hydraulic actuation system of clutch C2 and power-train.

### 2.1 Engine dynamic model

Considering the response time of engine, the engine output torque can be modelled by a first-order process:

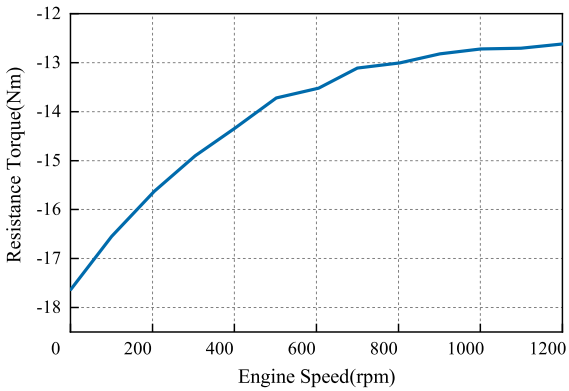


**Fig. 2** Engine friction torque

$$T_{\text{en}} = \frac{1}{\tau_{\text{en}} \cdot s + 1} T_{\text{en\_cmd}} \tag{1}$$

During the engine start process, engine is started by motor 1, so engine is a load driven by motor 1. The drag characteristics can be modelled according to [26], as shown in Fig. 2.

$$T_{\text{en\_fric}} = f(n_{\text{en}}) \tag{2}$$

## 2.2 Motor dynamic model

Motor 1 is used as auxiliary motor with peak torque of 160 Nm and peak power of 55 kW. And motor 2 is used as main motor with peak torque of 155 Nm and peak power of 70 kW. The dynamic characteristics of motor can also be modelled according to the experimental data, as shown in Figs. 3 and 4. Similarly, considering the response time of motor, the motor output torque can be modelled as

$$\begin{cases} T_{\text{m1}} = \frac{1}{\tau_{\text{m1}} \cdot s + 1} f\left(T_{\text{m1\_cmd}}, n_{\text{m1}}\right) \\ T_{\text{m2}} = \frac{1}{\tau_{\text{m2}} \cdot s + 1} f\left(T_{\text{m2\_cmd}}, n_{\text{m2}}\right) \end{cases} \tag{3}$$

## 2.3 Wet clutch actuating system model

The wet clutch C2 is adopted to transfer the torque of engine and motor 1 in hybrid driving mode. The schematic of its actuating system is shown in Fig. 5, which mainly consists of one piston, steel plate, friction plate, reset spring and high pressure oil. The flow of high pressure oil is adjusted by a high speed on-off valve. The piston moves as the pressure of oil increases, thus eliminates the gap between steel plate and friction

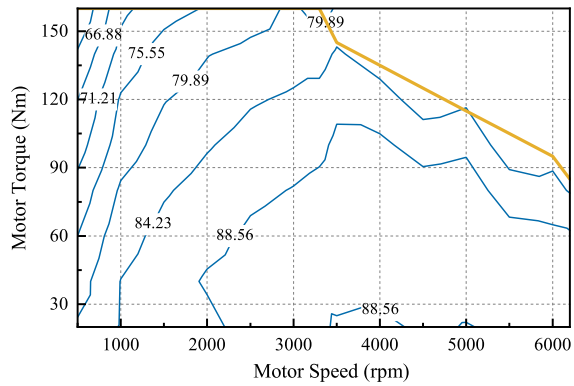


**Fig. 3** Dynamic characteristics Map of motor 1

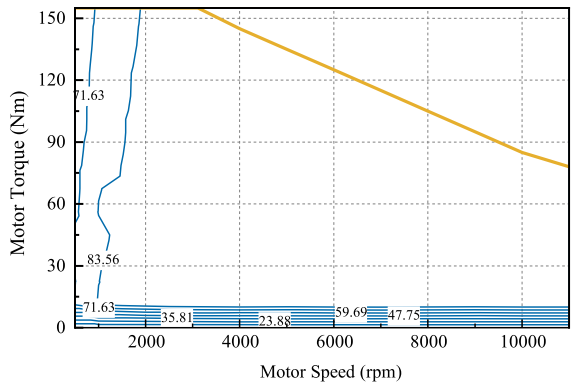


**Fig. 4** Dynamic characteristics Map of motor 2

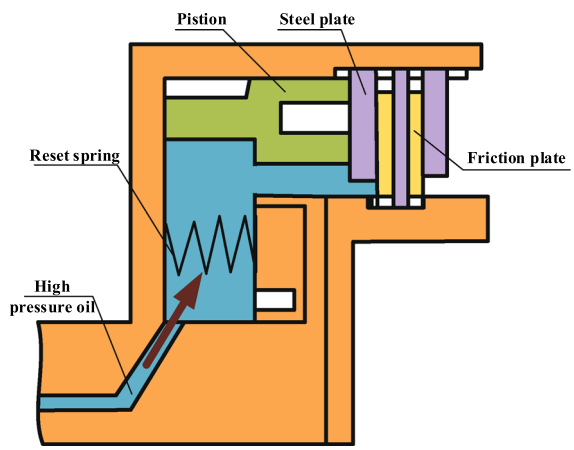


**Fig. 5** Schematic of wet clutch C2

plate. Reset spring is used to prevent the possibly pressure on plates without oil pressure. When the clutch is released, the torque transmitted by it is zero. And when the wet clutch is fully engaged, if the combined force of the engine and the motor is less than the maximum

force that the clutch can transmit, then the force transmitted by the clutch is equal to the combined force, otherwise the output is the maximum torque that the clutch can transmit. In order to simulate the nonlinear dynamic characteristics of clutch, the motion equation of the hydraulic actuator is given according to [27].

When the displacement $x_{\mathrm{p}}$ of piston achieves the maximum value $s$, the gap between steel plate and friction plate is eliminated. The clutch motion equation can be expressed as

$$k_p\left(x_{\mathrm{p0}}+s_{\max}\right)=F_p-F_{\mathrm{cl}} \tag{4}$$

The clutch tube fluid continuity equation is

$$Q_{\mathrm{c}}=\frac{(A_{C2}x_{\max}+V_0)\dot{P}_c}{\beta} \tag{5}$$

The average flow of the inlet opening of valve is

$$\tilde{Q}_{\mathrm{in}}=\tau C_h A_h\sqrt{\frac{2(P_s-P_c)}{\rho}} \tag{6}$$

The average flow of the outlet opening of valve is

$$\tilde{Q}_{\mathrm{out}}=(1-\tau)C_h A_h\sqrt{\frac{2(P_s-P_0)}{\rho}} \tag{7}$$

So the flow through the clutch tube can be considered as

$$Q_{\mathrm{c}}=\tilde{Q}_{\mathrm{in}}-\tilde{Q}_{\mathrm{out}} \tag{8}$$

The high speed on-off valve is controlled by pulse width modulation(PWM) control. In order to accurately control the torque transmitted by wet clutch C2, the duty ratio of PWM for the high speed on-off valve is needed to be controlled precisely. In this paper, the torque transmitted by clutch is controlled by a PID controller:

$$\tau=K_p\Delta T_{\mathrm{cl}}+K_I\int_k^{k+1}\Delta T_{\mathrm{cl}}+K_D\Delta\dot{T}_{\mathrm{cl}} \tag{9}$$

### 2.4 Power-train dynamic model

Ignoring the planetary gear and the damping of each component, it is assumed that the components in the power system are rigid bodies, and the concentrated inertia at the nodes is used to represent the rotational inertia of each component [11]. The structure of DM-PHEV can be simplified as shown in Fig. 6.

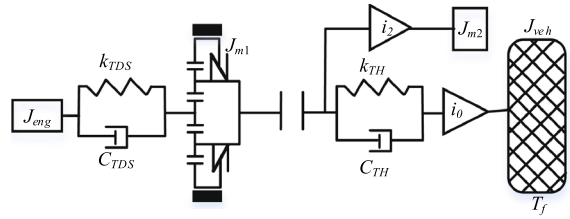


**Fig. 6** Planetary-wheel drive dynamics model

The kinematic equations of the PHEV are given by:

$$\begin{cases} T_{\mathrm{en}}-J_{\mathrm{en}}\dot{\omega}_{\mathrm{en}}=T_{\mathrm{TDS}} \\ T_{\mathrm{TDS}}=k_{\mathrm{TDS}}(\theta_{\mathrm{en}}-\theta_{\mathrm{TDS}})+C_{\mathrm{TDS}}(\dot{\theta}_{\mathrm{en}}-\dot{\theta}_{\mathrm{TDS}}) \\ T_{\mathrm{cl}}=T_{\mathrm{TDS}}+T_{\mathrm{m1}}-J_{\mathrm{m1}}\ddot{\theta}_l \\ i_2(T_{\mathrm{m2}}-J_{\mathrm{m2}}i_2\ddot{\theta}_r)+T_{\mathrm{cl}}=T_{\mathrm{TH}} \\ T_{\mathrm{TH}}=k_{\mathrm{TH}}\left(\theta_r-i_0\theta_f\right)+C_{\mathrm{TH}}\left(\dot{\theta}_r-i_0\dot{\theta}_f\right) \\ T_{\mathrm{TH}}i_0-T_f=J_{\mathrm{veh}}\ddot{\theta}_f \end{cases} \tag{10}$$

The driving resistance of vehicle includes the rolling resistance, air resistance, acceleration resistance and climbing resistance, thus can be expressed as [28]

$$\frac{T_f\eta_t}{R}=\frac{C_{\mathrm{d}}A}{21.15}v^2+m_{\mathrm{veh}}gf\cos\alpha+m_{\mathrm{veh}}g\sin\alpha \tag{11}$$

where $T_{\mathrm{cl}}$ depends on the state of clutch C2, as shown in wet clutch actuator system model.

## 3 Hybrid model of DM-PHEV

### 3.1 Problem description of mode transition process

Once the energy management controller requires the vehicle to enter hybrid driving mode to acquire best fuel economy, then DM-PHEV runs into mode transition process. As shown in Fig. 7, the mode transition process from EM to HM can be divided into 5 stages. In Stage 1, the DM-PHEV is propelled by motor 2. In Stage 2, engine is cranked up rapidly by motor 1, and is ignited when the engine speed exceeds the idle speed. Clutch C2 keeps released to avoid the transmission of engine ripple torque to power-train, so DM-PHEV is still propelled by motor 2. Then if the speed of clutch driven disc on the engine side is smaller than the speed of clutch driving disc, the mode transition process enters stage 3. During this stage, Motor 1 drives the clutch driving disc until the clutch driven disc speed $\omega_l$ and the clutch driving disc speed $\omega_r$ satisfy $\omega_l-\omega_r>a$, where $a$ is a certain limit, then mode transition process runs into Stage 4. In Stage 4, clutch C2 begins to slip,

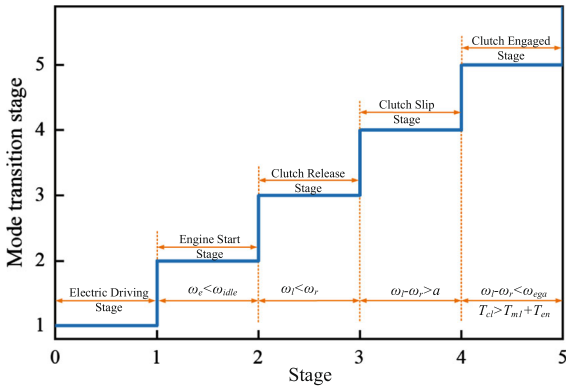


**Fig. 7** Mode transition process of DM-PHEV

and motor 1 and clutch C2 work together to reduce the speed difference between the two ends of clutch. Meanwhile, Motor 2 and clutch C2 propelled the DM-PHEV together.

When the speed difference between the left and right sides of the clutch is less than a certain limit $\omega_{\text{ega}}$ and the torque that the clutch can transmit is greater than the combined force of the engine and the motor 1, the clutch starts to engage and mode transition process enters into stage 5. the torque transmitted by the clutch at this stage is equal to the combined force of the engine and the motor 1, so engine, motor 1 and motor 2 work together to drive the vehicle.

As the mode transition process consists of five stages, and each stage has its own cost function. The main novelty here is adopting the Mixed-Logic Dynamic(MLD) formulation to build the DM-PHEV dynamic model. MLD systems allows the continuous variables evolutes through linear affine equations, and Boolean variables are used to represent the threshold conditions of continuous variables.

The form of the MLD model is shown in Eq. (12) [29]. The first two equations of Eq. (12) are linear, and the nonlinearity of system is hidden in the inequalities, which help transform the system contains logic part into mixed-integer linear inequalities.

$$\begin{aligned} x(k+1) &= Ax(k) + B_1u(k) + B_2\delta(k) + B_3z(k) \\ y(k) &= Cx(k) + D_1u(k) + D_2\delta(k) + D_3z(k) \\ E_2\delta(k) + E_3z(k) &\le E_4x(k) + E_1u(k) + E_5 \end{aligned} \tag{12}$$

Where $k$ is the discrete time-instant; $x(k)$ denotes the states; $x(k) = \left[\Delta w_l(k)\ \Delta w_r(k)\ w_l(k)\ w_r(k)\right]$; u(k) denotes the inputs, $u(k) = \left[T_{\text{m1}}\ T_{\text{m2}}\ T_{\text{cl}}\right]$; y(k) denotes the outputs, $y(k) = x(k)$; Besides, $\delta$ and $z$ are the binary and auxiliary continuous variables, respectively, which are introduced to translate the piecewise affine systems(PWA) functions into linear inequalities.

To acquire MLD model of DM-PHEV, discrete time linear affine system model should to be constructed firstly.

### 3.2 System state equations of power-train during mode transition

Combined with the power-train mathematical models shown in Table 1, the state variables are selected as

$$x_1 = w_l, x_2 = w_r \tag{13}$$

and the control variables are selected as

$$u_1 = T_{\text{m1}}, u_2 = T_{\text{m2}}, u_3 = T_{\text{cl}} \tag{14}$$

The compound power-split PHEV state equations can be represented by the following equation

$$\dot{x} = Ax + Bu + C \tag{15}$$

The HC-MPC controller requires a linear model, while the driving resistance contains ${\omega_r}^2$, which is a nonlinear part, so Taylor series expansion is used

$$\begin{aligned} [\omega_r(k)]^2 = {} & [\omega_r(k-1)]^2 \\ & +2\omega_r(k-1)\left[\omega_r(k) - \omega_r(k-1)\right] \end{aligned} \tag{16}$$

For time $k$, the state at time $k-1$ is known, so $\omega_r(k-1)$ can be regarded as a constant, thus Eq. (16) can be transformed into

$$[\omega_r(k)]^2 = M^2 + 2M\left[\omega_r(k) - M\right] \tag{17}$$

Then, at each step ${\omega_r}^2$ can be transformed as a linear function.

The nonlinear engine resistance torque model is approximated as a piecewise affine function of engine speed by using the least square method, as shown in Fig. 8. Linear engine resistance torque is

$$T_{\text{en\_fri}} = \begin{cases} 0.0078n_{\text{en}} - 17.3995 & n_{\text{en}} \le 507 \\ 0.0014n_{\text{en}} - 14.1573 & 507 \le n_{\text{en}} \le 800 \end{cases} \tag{18}$$

Continuous model in Eq. (15) is discretized with sampling time $T_s = 10$ ms. The state increment and control increment are defined as

$$\begin{cases} \Delta x(k) = x(k) - x(k-1) \\ \Delta u(k) = u(k) - u(k-1) \end{cases} \tag{19}$$

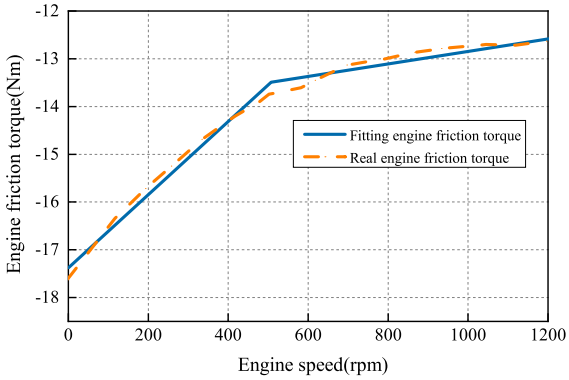


**Fig. 8** Linearisation of engine friction torque

Thus, the state equation can be converted to:

$$\begin{bmatrix} \Delta x_1(k+1) \\ \Delta x_2(k+1) \end{bmatrix} = A \begin{bmatrix} \Delta x_1(k) \\ \Delta x_2(k) \end{bmatrix} + B \begin{bmatrix} \Delta u_1(k) \\ \Delta u_2(k) \\ \Delta u_3(k) \end{bmatrix} \tag{20}$$

To constraint the derivative of torque and eliminate static errors, a new state vector is selected as:

$$\tilde{x}(k) = \begin{bmatrix} \Delta x_1(k) \\ \Delta x_2(k) \\ x_1(k) \\ x_2(k) \end{bmatrix} \tag{21}$$

The stage space equation can be further transformed to

$$\begin{cases} \tilde{x}(k+1) = \tilde{A}\tilde{x}(k) + \tilde{B}\Delta u(k) \\ \tilde{A} = \begin{bmatrix} A & 0 \\ A & E \end{bmatrix} \\ \tilde{B} = \begin{bmatrix} B \\ B \end{bmatrix} \end{cases} \tag{22}$$

The coefficient matrix of the state equations at each stage is shown in Table 1.

**Table 1** Description of mode transition process

| Stage | Power-train mathematical models | Stage | Power-train mathematical models |
|---|---|---|---|
| Stage 1 | $\tilde{A}_1 = \begin{bmatrix} 0 & 0 & 0 & 0 \\ 0 & 1-\frac{2\Delta t C_d A}{21.15\eta_t i_0^3 J_{re}} R^3 M & 0 & 0 \\ 0 & 0 & 0 & 0 \\ 0 & 1-\frac{2\Delta t C_d A}{21.15\eta_t i_0^3 J_{re}} R^3 M & 0 & 1 \end{bmatrix}$, $\tilde{B}_1 = \begin{bmatrix} 0 & 0 & 0 \\ 0 & \frac{i_2\Delta t}{J_{re}} & 0 \\ 0 & 0 & 0 \\ 0 & \frac{i_2\Delta t}{J_{re}} & 0 \end{bmatrix}$ | Stage 2 | $\tilde{A}_2 = \begin{bmatrix} 1+\frac{A_{fric}\cdot\Delta t}{J_{le}} & 0 & 0 & 0 \\ 0 & 1-\frac{2\Delta t C_d A}{21.15\eta_t i_0^3 J_{re}} R^3 M & 0 & 0 \\ 1+\frac{A_{fric}\cdot\Delta t}{J_{le}} & 0 & 1 & 0 \\ 0 & 1-\frac{2\Delta t C_d A}{21.15\eta_t i_0^3 J_{re}} R^3 M & 0 & 1 \end{bmatrix}$, $\tilde{B}_2 = \begin{bmatrix} \frac{\Delta t}{J_{le}} & 0 & 0 \\ 0 & \frac{i_2\Delta t}{J_{re}} & 0 \\ \frac{\Delta t}{J_{le}} & 0 & 0 \\ 0 & \frac{i_2\Delta t}{J_{re}} & 0 \end{bmatrix}$ |
| Stage 3 | $\tilde{A}_3 = \begin{bmatrix} 1 & 0 & 0 & 0 \\ 0 & 1-\frac{2\Delta t C_d A}{21.15\eta_t i_0^3 J_{re}} R^3 M & 0 & 0 \\ 1 & 0 & 1 & 0 \\ 0 & 1-\frac{2\Delta t C_d A}{21.15\eta_t i_0^3 J_{re}} R^3 M & 0 & 1 \end{bmatrix}$, $\tilde{B}_3 = \begin{bmatrix} \frac{\Delta t}{J_{le}} & 0 & 0 \\ 0 & \frac{i_2\Delta t}{J_{re}} & 0 \\ \frac{\Delta t}{J_{le}} & 0 & 0 \\ 0 & \frac{i_2\Delta t}{J_{re}} & 0 \end{bmatrix}$ | Stage 4 | $\tilde{A}_4 = \begin{bmatrix} 1 & 0 & 0 & 0 \\ 0 & 1-\frac{2\Delta t C_d A}{21.15\eta_t i_0^3 J_{re}} R^3 M & 0 & 0 \\ 1 & 0 & 1 & 0 \\ 0 & 1-\frac{2\Delta t C_d A}{21.15\eta_t i_0^3 J_{re}} R^3 M & 0 & 1 \end{bmatrix}$, $\tilde{B}_4 = \begin{bmatrix} \frac{\Delta t}{J_{le}} & 0 & -\frac{\Delta t}{J_{le}} \\ 0 & \frac{i_2\Delta t}{J_{re}} & \frac{\Delta t}{J_{re}} \\ \frac{\Delta t}{J_{le}} & 0 & -\frac{\Delta t}{J_{le}} \\ 0 & \frac{i_2\Delta t}{J_{re}} & \frac{\Delta t}{J_{re}} \end{bmatrix}$ |
| Stage 5 | $\tilde{A}_5 = \begin{bmatrix} 0 & 1-\frac{2\Delta t C_d A}{21.15\eta_t i_0^3 (J_{le}+J_{re})} R^3 M & 0 & 0 \\ 0 & 1-\frac{2\Delta t C_d A}{21.15\eta_t i_0^3 (J_{le}+J_{re})} R^3 M & 0 & 0 \\ 0 & 1-\frac{2\Delta t C_d A}{21.15\eta_t i_0^3 (J_{le}+J_{re})} R^3 M & 0 & 1 \\ 0 & 1-\frac{2\Delta t C_d A}{21.15\eta_t i_0^3 (J_{le}+J_{re})} R^3 M & 0 & 1 \end{bmatrix}$, $\tilde{B}_5 = \begin{bmatrix} \frac{\Delta t}{J_{le}+J_{re}} & \frac{i_2\Delta t}{J_{le}+J_{re}} & 0 \\ \frac{\Delta t}{J_{le}+J_{re}} & \frac{i_2\Delta t}{J_{le}+J_{re}} & 0 \\ \frac{\Delta t}{J_{le}+J_{re}} & \frac{i_2\Delta t}{J_{le}+J_{re}} & 0 \\ \frac{\Delta t}{J_{le}+J_{re}} & \frac{i_2\Delta t}{J_{le}+J_{re}} & 0 \end{bmatrix}$ | | |

where $\begin{cases} M = (\omega_r(k))^2 \\ J_{le} = J_{en} + J_{m1} + J_p \\ J_{re} = J_{m2} i_2{}^2 + J_r + \frac{J_{veh}}{i_0{}^2} \end{cases}$

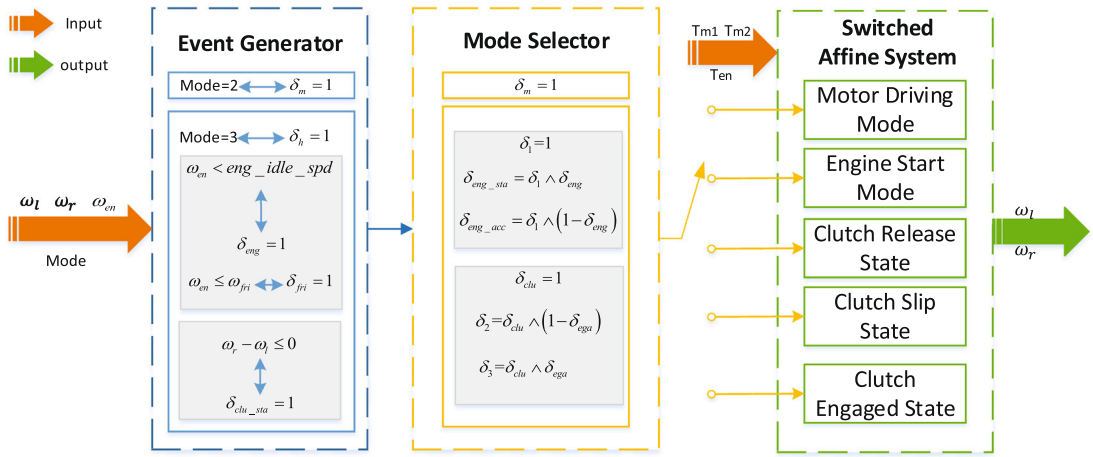


**Fig. 9** Mode transition MLD model

## 3.3 Modelling of PHEV system based on hybrid system theory

The discrete-time MLD model is based on the discrete dynamic model of DM-PHEV. As shown in Fig. 9, the PHEV MLD system can be divided into three subsections. Event generator receives the actual states of DM-PHEV and converts the relationships between the states into binary auxiliary variables. These binary variables will be sent to Mode Selector. Mode Selector further judges the stage of mode transition process according to the binary variables and generate new binary variables to represent the current stage. According to the rules of MLD, these logic equations will be transformed into inequalities and equalities. Finally, the mode binary variables are combined with state-space equations of each stage. Auxiliary continuous variables are introduced to represent the states of DM-PHEV in each stage.

### *3.3.1 Event generator*

An event generator is to generate some binary signals $\delta \in \{0, 1\}$ according to the satisfaction of some linear constraints.

Considering the PHEV system, auxiliary variables $\delta_m$ and $\delta_h$ are associated with vehicle driving mode. If vehicle is driving in electric driving stage, then $\delta_m = 1$, otherwise $\delta_m = 0$; If vehicle is driving in hybrid driving stage, then $\delta_h = 1$, otherwise $\delta_h = 0$.

According to the five stages proposed before, if $\omega_r - \omega_l \leq 0$, then clutch may start to slip, which is connected with an auxiliary variable $\delta_{\text{clu\_sta}}$.

$$\omega_r - \omega_l \leq 0 \leftrightarrow \delta_{\text{clu\_sta}} = 1 \tag{23}$$

As described in [29], by adopting the so-called big-M technique, the logic equation can be equivalently expressed as

$$\begin{cases} -m\delta_{\text{clu\_sli}} \leq \omega_l - \omega_r - m \\ (-M - \varepsilon)\delta_{\text{clu\_sli}} \leq \omega_r - \omega_l - \varepsilon \end{cases} \tag{24}$$

where $M \triangleq \max_{x\in\partial} f(x)$, $m \triangleq \min_{x\in\partial} f(x)$, $\partial$ is the given bounded set, and $\varepsilon$ is a small positive scalar.

If engine speed is lower than engine idle speed $n_{\text{idle}}$, it means that PHEV is in engine start stage, which is connected with binary variable $\delta_{\text{eng}}$.

$$\begin{aligned} & x_1 < n_{\text{idle}} \leftrightarrow \delta_{\text{eng}} = 1 \\ & \Leftrightarrow \begin{cases} \omega_l + (M - n_{\text{idle}})\delta_{\text{eng}} \leq M \\ (m - \varepsilon - n_{\text{idle}})\delta_{\text{eng}} - \omega_l \leq -n_{\text{idle}} - \varepsilon \end{cases} \end{aligned} \tag{25}$$

Based on the engine resistance piecewise linear (PWA) model in Eq. (31), auxiliary discrete variable $\delta_{\text{fri}}$ is defined as

$$\begin{aligned} & n_{\text{en}} \leq n_{\text{thresh}} \leftrightarrow \delta_{\text{fri}} = 1 \\ & \Leftrightarrow \begin{cases} n_{\text{en}} + (M - n_{\text{thresh}})\,\delta_{\text{fri}} \leq M \\ (m - \varepsilon - n_{\text{thresh}})\,\delta_{\text{fri}} - n_{\text{en}} \leq -n_{\text{thresh}} - \varepsilon \end{cases} \end{aligned} \tag{26}$$

When the speed difference between the driven and driving disc of the clutch is less than a constant $\omega_{\text{ega}}$ and the torque that can be transmitted during slipping

is bigger than the combined force of the engine and the motor 1, the clutch can be considered to be engaged. Two auxiliary variables are used to represent this condition

$$\begin{aligned} &T_{\text{en}} + T_{\text{m1}} - T_{\text{cl}} \le T_{\text{ega}} \leftrightarrow \delta_{T_{\text{ega}}} = 1 \\ &\Leftrightarrow \begin{cases} T_{\text{err}} = T_{\text{en}} + T_{\text{m1}} - T_{\text{cl}} \\ (M - T_{\text{ega}})\delta_{T_{\text{ega}}} \le M + T_{\text{err}} \\ (m - \varepsilon - T_{\text{ega}})\delta_{T_{\text{ega}}} \le T_{\text{err}} - T_{\text{ega}} + \varepsilon \end{cases} \end{aligned} \tag{27}$$

$$\begin{aligned} &\omega_l - \omega_r - \omega_{\text{ega}} \le 0 \leftrightarrow \delta_{\omega_{\text{ega}}} = 1 \\ &\Leftrightarrow \begin{cases} \omega_l - \omega_r \le (M - \omega_{\text{ega}})(1 - \delta_{\omega_{\text{ega}}}) + \omega_{\text{ega}} \\ \omega_l - \omega_r \ge \omega_{\text{ega}} + \varepsilon + (m - \varepsilon - \omega_{\text{ega}})\delta_{\omega_{\text{ega}}} \end{cases} \end{aligned} \tag{28}$$

### 3.3.2 Mode selector

The dynamic mode of system is selected through mode selector.

The coordinated control system switches between five subsystems, and the logical variable $\delta_i$ is defined to represent the $i$-th subsystem. The binary auxiliary variables introduced in the last section can be used to determine the mode of PHEV system. $\delta_i = 1$ means the state of PHEV system is in Stage $i$.

If $\delta_m = 1$, then there is no doubt that PHEV is in electric driving stage. If PHEV is in hybrid driving mode, and the auxiliary variable $\delta_{\text{clu\_sta}} = 1$ is satisfied, then it means that clutch starts to act on the system.

$$\begin{aligned} &(\delta_h = 1) \wedge \left(\delta_{\text{clu\_sta}} = 1\right) \leftrightarrow \delta_{\text{clu}} = 1 \\ &\Leftrightarrow \begin{cases} -\delta_h + \delta_{\text{clu}} \le 0 \\ -\delta_{\text{clu\_sta}} + \delta_{\text{clu}} \le 0 \\ \delta_h + \delta_{\text{clu\_sta}} - \delta_{\text{clu}} \le 1 \end{cases} \end{aligned} \tag{29}$$

The stage before clutch slipping stage can be defined by auxiliary variable $\delta_1 = 1$.

$$\delta_1 + \delta_{\text{clu}} + \delta_m = 1 \tag{30}$$

Furthermore, the engine start stage can be defined as

$$\begin{aligned} &\delta_{\text{eng\_sta}} = \delta_1 \wedge \delta_{\text{eng}} \\ &\Leftrightarrow \begin{cases} -\delta_1 + \delta_{\text{eng\_sta}} \le 0 \\ -\delta_{\text{eng}} + \delta_{\text{eng\_sta}} \le 0 \\ -\delta_{\text{eng}} + \delta_{\text{eng\_sta}} \le 0 \end{cases} \end{aligned} \tag{31}$$

Clutch release stage can be defined as

$$\begin{aligned} &\delta_{\text{eng\_acc}} = \delta_1 \wedge \left(1 - \delta_{\text{eng}}\right) \\ &\Leftrightarrow \begin{cases} -\delta_1 + \delta_{\text{eng\_acc}} \le 0 \\ \delta_{\text{eng}} + \delta_{\text{eng\_acc}} \le 1 \\ \delta_1 - \delta_{\text{eng}} - \delta_{\text{eng\_acc}} \le 0 \end{cases} \end{aligned} \tag{32}$$

The criterion for judging whether the clutch is engaged is that the speed difference between the two ends is small enough and the clutch torque is greater than the combined force of the engine and the motor 1. So binary variable $\delta_{\text{ega}}$ is defined as

$$\begin{aligned} &\delta_{\text{ega}} = \delta_{T_{\text{ega}}} \wedge \delta_{\omega_{\text{ega}}} \\ &\Leftrightarrow \begin{cases} -\delta_{T_{\text{ega}}} + \delta_{\text{ega}} \le 0 \\ -\delta_{\omega_{\text{ega}}} + \delta_{\text{ega}} \le 0 \\ \delta_{T_{\text{ega}}} + \delta_{\omega_{\text{ega}}} - \delta_{\text{ega}} \le 1 \end{cases} \end{aligned} \tag{33}$$

The slip and engagement state of the clutch can be defined as

$$\begin{aligned} &\delta_2 = \delta_{\text{clu}} \wedge \left(1 - \delta_{\text{ega}}\right) \\ &\Leftrightarrow \begin{cases} -\delta_{\text{clu}} + \delta_2 \le 0 \\ \delta_{\text{ega}} + \delta_2 \le 1 \\ \delta_{\text{clu}} - \delta_{\text{ega}} - \delta_2 \le 0 \end{cases} \end{aligned} \tag{34}$$

$$\begin{aligned} &\delta_3 = \delta_{\text{clu}} \wedge \delta_{\text{ega}} \\ &\Leftrightarrow \begin{cases} -\delta_{\text{clu}} + \delta_3 \le 0 \\ -\delta_{\text{ega}} + \delta_3 \le 0 \\ \delta_{\text{clu}} + \delta_{\text{ega}} - \delta_3 \le 1 \end{cases} \end{aligned} \tag{35}$$

### 3.3.3 Switched affine system

The continuous dynamics change with the mode which is generated by the mode selector, and it can be modelled by a discrete-time switched affine system (SAS).

For PHEV system, its state equations is determined by the mode $\delta_i$ as shown in Section A, which is a typical SAS, to translate the SAS into equivalent mixed-integer linear inequalities, set auxiliary continuous $z_i$ as

$$z_i = \left(\tilde{A}_i x + \tilde{B}_i u\right)\delta_i \tag{36}$$

$$x\,(k+1) = \sum_{i=1}^{5} z_i \tag{37}$$

For the engine resistance torque model, set auxiliary continuous $z_{\text{fric}}$ as

$$\begin{cases} z_{\text{fric1}} = \left(1 + \frac{A_{\text{fric1}} \cdot \Delta t}{J_{le}}\right) x_1 \cdot \delta_{\text{fri}} \\ z_{\text{fric2}} = \left(1 + \frac{A_{\text{fric2}} \cdot \Delta t}{J_{le}}\right) x_1 \cdot (1 - \delta_{\text{fri}}) \end{cases} \tag{38}$$

Then, the coefficient $(1 + A_{\text{fri}})$ in Table 1 can be rewritten as

$$\left(1 + \frac{A_{\text{fric}} \cdot \Delta t}{J_{le}}\right) x_1 = z_{\text{fric1}} + z_{\text{fric2}} \tag{39}$$

Logical equation from Eq. (36) to Eq. (38) can be transformed into following inequalities

$$\begin{cases} z_i - M_x(i,1)\,\delta_i \le 0 \\ -z_i + m_x(i,1)\,\delta_i \le 0 \\ z_i - m_x(i,1)\,\delta_i \le \tilde{A}_i\tilde{x} + \tilde{B}_i\Delta u - m_x(i,1) \\ -z_i + M_x(i,1)\,\delta_i \le -\tilde{A}_i\tilde{x} - \tilde{B}_i\Delta u + M_x(i,1) \end{cases} \tag{40}$$

*3.3.4 Physical constraints*

There are physical constraints on the motor and clutch. The following constraints on the torque need to be satisfied

$$\begin{cases} T_{\mathrm{m1\_min}} \le u_1 \le T_{\mathrm{m1\_max}} \\ T_{\mathrm{m2\_min}} \le u_2 \le T_{\mathrm{m2\_max}} \\ T_{cl\_min} \le u_3 \le T_{cl\_max} \\ \Delta T_{\mathrm{m1\_min}} \le \Delta u_1 \le \Delta T_{\mathrm{m1\_max}} \\ \Delta T_{\mathrm{m2\_min}} \le \Delta u_2 \le \Delta T_{\mathrm{m2\_max}} \\ \Delta T_{\mathrm{m3\_min}} \le \Delta u_3 \le \Delta T_{\mathrm{m3\_max}} \end{cases} \tag{41}$$

Finally, the inequalities and equalities transformed before can be summarized as Eq. (12).

## 4 Coordinated control of DM-PHEV

### 4.1 Coordinated control objectives and control architecture

The main objectives of coordinated control can be described as follows:

1. Driver demand guarantee: In order to guarantee the torque demand of driver, the torque distribution of power sources should be considered in coordinated control strategy.
2. Ride comfort of passengers: To reduce the torque fluctuation during mode transition process, the nonlinear dynamic characteristics of clutch and torque compensation from motors need to be considered. This study use vehicle jerk $j$ as the evaluation index for driving comfort.

$$j = \dot{a} = \ddot{v} \tag{42}$$

3. Minimize energy consumption: The mode transition of DM-PHEV has clutch engagement process, so clutch slipping energy loss is also considered to minimize energy consumption and prolong clutch service life. Clutch slipping energy $W$ is considered as

$$W = \int_{t_0}^{t_f} T_{\mathrm{cl}}(\omega_l - \omega_r)\mathrm{d}t \tag{43}$$

To acquire best mode transition performance, a coordinated control strategy based on the MLD model built in Sect. 2.1 is developed. As shown in Fig. 10, the control strategy can be divided into five main parts: (1) Reference model for MPC which is different for each stage; (2) Stage Judgement which is part of MLD model built in Sect. 2.1; (3) MLD model which is used to predict the state of DM-PHEV in the next several step; (4) Variable cost function which can unify the different reference model for each stage; (5) MILP problem: the MPC controller based on MLD can be transformed as a MILP problem which can be solved by MATLAB toolbox.

### 4.2 H-MPC based on MLD

In this section, hybrid MPC controller(H-MPC) [24, 30,31] is adopted as coordinate controller using MLD model which is built in Sect. 2.1. As the MLD model is unified for the whole mode transition process, only one controller is used as coordinate controller, which can prevent instability caused by switching between multiple controllers. Similar to the traditional MPC control algorithm, the main idea of H-MPC is using the MLD model to predict evolution of PHEV system in the next few steps. In this study, the states predicted by MPC are the speeds of clutch driven disc and driving disc. Then, the coordinated control problem can be transformed into the problem of tracking the reference speed at both ends of the clutch. Besides,by minimizing the fluctuation of vehicle driving torque and accelerating the speed tracking process, the coordinated controller can prevent vehicle jerk and reduce clutch slipping energy loss at the same time. A certain performance index is optimized at each time step, which converting the mode switching coordination control to finite horizon optimal control problem. Then, an optimized control sequence is solved to minimize the value of the performance index. Only the first control action will be applied to the system at time $t$, and a new optimization will be solved at time $t$+1 over a shifted prediction horizon. For the mode transition process of DM-PHEV system, the following finite horizon optimal control problem is solved at each time step

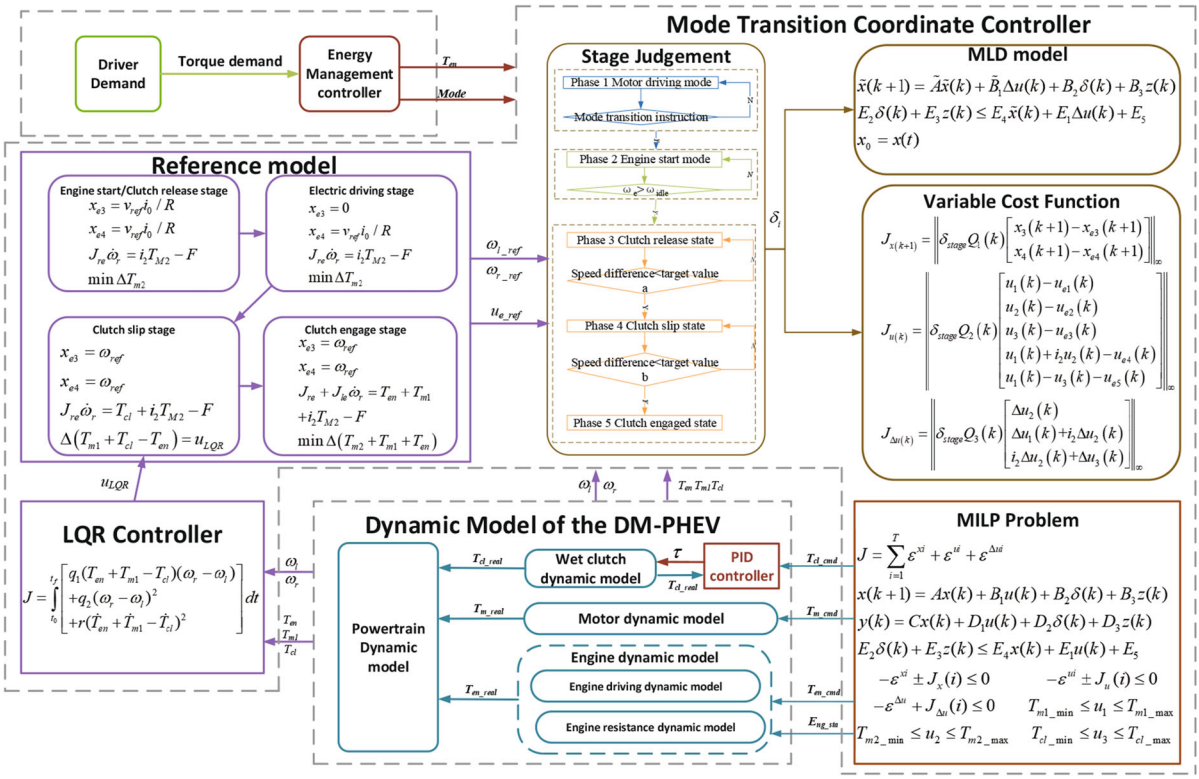


**Fig. 10** Coordinate control architecture

$$\min_{\{x_e,u_e\}} \sum_{k=0}^{T-1} \left( J_{x(k+1|t)} + J_{u(k|t)} + J_{\Delta u(k|t)} \right) \tag{44}$$

$$\begin{cases} \tilde{x}(k+1) = \tilde{A}\tilde{x}(k) + \tilde{B}_1 \Delta u(k) + B_2 \delta(k) + B_3 z(k) \\ E_2 \delta(k) + E_3 z(k) \le E_4 \tilde{x}(k) + E_1 \Delta u(k) + E_5 \\ x_0 = x(t) \end{cases} \tag{45}$$

where

$$\begin{cases} J_{x(k+1)} = \left\| Q_1(k) \begin{bmatrix} x_3(k+1) - x_{e3}(k+1) \\ x_4(k+1) - x_{e4}(k+1) \end{bmatrix} \right\|_\infty \\ J_{u(k)} = \left\| Q_2(k) \begin{bmatrix} u_1(k) - u_{e1}(k) \\ u_2(k) - u_{e2}(k) \\ u_3(k) - u_{e3}(k) \\ u_1(k) + i_2 u_2(k) - u_{e4}(k) \\ u_1(k) - u_3(k) - u_{e5}(k) \end{bmatrix} \right\|_\infty \\ J_{\Delta u(k)} = \left\| Q_3(k) \begin{bmatrix} \Delta u_2(k) \\ \Delta u_1(k) + i_2 \Delta u_2(k) \\ i_2 \Delta u_2(k) + \Delta u_3(k) \end{bmatrix} \right\|_\infty \end{cases} \tag{46}$$

The cost function of H-MPC can be divided into three parts. $J_x$ is used to represent the error between reference speed and actual speed of clutch discs to realize the fast engagement of clutch and the tracking of driver desired speed. $J_u$ is used to meet the torque demand of driver. And $J_{\Delta u}$ is to limit the torque changing rate of DM-PHEV for different stages.

Finally, Eqs. (44) and (45) can be translated into a mixed integer linear program(MILP) optimal problem.

Let

$$J = \min \sum_{i=1}^{T} \varepsilon^{xi} + \varepsilon^{ui} + \varepsilon^{\Delta ui} \tag{47}$$

denote the value function corresponding to Eq. (44), where $\varepsilon$ is auxiliary variable which is subject to

$$\begin{cases} -\varepsilon^{xi} \pm Q_1(x_i - x_{ei}) \le 0 \\ -\varepsilon^{ui} \pm Q_2(u_i - u_{ei}) \le 0 \\ -\varepsilon^{\Delta ui} \pm Q_3 \Delta u_i \le 0 \end{cases} \tag{48}$$

By computing such a MILP problem, the resulting control law is

$$\begin{cases} T_{\mathrm{m1}}(k+1) = T_{\mathrm{m1}}(k) + \Delta u_1(k) \\ T_{\mathrm{m2}}(k+1) = T_{\mathrm{m2}}(k) + \Delta u_2(k) \\ T_{\mathrm{cl}}(k+1) = T_{\mathrm{cl}}(k) + \Delta u_3(k) \end{cases} \tag{49}$$

As shown in Eq. (46), a reference model is needed in cost functions. For the coordinated controller, refer-

ence model changes with the stage of mode transition process.

#### 4.2.1 Control objectives in stage 1

Motor 2 drives the vehicle in Stage 1, motor 1 and clutch do not work. The control objective is to meet the driver demand via torque of motor 2 and minimize the vehicle jerk by limiting the torque changing rate of motor 2.

$$j = \frac{i_2 \dot{T}_{\mathrm{m2}} - \dot{T}_f}{i_0 j_{re}} R \tag{50}$$

Driver demand torque and reference speed can be calculated from

$$\begin{cases} J_{re}\dot{\omega}_r = i_2 T_{\mathrm{m2}} - F \\ \omega_{l\_ref} = 0 \\ \omega_{r\_ref} = \frac{v_{\mathrm{ref}} i_0}{R} \end{cases} \tag{51}$$

where

$$F = \frac{C_{\mathrm{d}} A}{21.15 \eta_t i_0} R^3 {\omega_r}^2 - \frac{mgfR}{\eta_t i_0} \tag{52}$$

#### 4.2.2 Control objectives in stage 2/3

In stage 2, engine needs to be started by motor 1, and in stage 3, the speed of clutch driven disc $\omega_l$ needs to be accelerated until satisfy $\omega_l - \omega_r > a$. So the control objectives can be summarized as motor 1 drives the driven disc of clutch to reference speed.

$$\omega_{l\_ref} = \frac{v_{\mathrm{ref}} i_0}{R} \tag{53}$$

As the clutch keeps released during this stage, so the vehicle jerk only depends on the torque changing rate of motor 2 which is similar to Stage 1.

#### 4.2.3 Control objectives in stage 4

In this stage, clutch C2 slips to smoothly connect the power sources of engine side and motor 2. The torque of engine, motor 1 and clutch act on the driven disc of clutch together to accelerate the slipping process of clutch. The object of this stage is to reduce the vehicle jerk while reducing the slipping energy of the clutch. The vehicle jerk in this stage is decided by the changing rate of the combined force of motor 2 and clutch.

$$j = \frac{i_2 \dot{T}_{\mathrm{m2}} + \dot{T}_{\mathrm{cl}} - \dot{T}_f}{i_0 j_{re}} R \tag{54}$$

From Eq. (43), it can be seen that the clutch slipping energy is consumed by the clutch during the entire slipping process. And in order to reduce the jerk happening in the end of slipping stage, the acceleration of the clutch driven disc should be closed to 0 at the moment of clutch engagement, which can ensure a little torque changing rate acts on vehicle.

Since MPC is optimized in a finite horizon, the global optimization algorithm LQR is used to optimize the torque during the clutch slipping process [32]. However, LQR has higher requirements on the accuracy of the model, so the combination of LQR and MPC is used in controller, the torque calculated by LQR is used as the reference of MPC.

LQR weight matrices are used to reflect the preference of two contradictory targets. According to the state equations of PHEV, the state variables are selected to represent the requirement of speed and torque, respectively.

$$\begin{cases} x_1 = w_r - w_l \\ x_2 = T_{\mathrm{en}} + T_{\mathrm{m1}} - T_{\mathrm{cl}} \end{cases} \tag{55}$$

Changing rate of the combined force of engine, motor and clutch is set as the control variable

$$u = \dot{T}_{\mathrm{en}} + \dot{T}_{\mathrm{m1}} - \dot{T}_{\mathrm{cl}} \tag{56}$$

So, the system state-space equation is

$$\dot{x} = Ax + Bu + C \tag{57}$$

where

$$A = \begin{bmatrix} 0 & -\frac{1}{j_{le}} \\ 0 & 0 \end{bmatrix}, B = \begin{bmatrix} 0 \\ 1 \end{bmatrix}, C = \begin{bmatrix} \dot{\omega}_r \\ 0 \end{bmatrix} \tag{58}$$

The cost function is shown in Eq. (59). $q$ reflects the intention of different objects.

$$J = \int_{t_0}^{t_f} \left[ q_1 T_{\mathrm{cl}} (\omega_l - \omega_r) + q_2 (\omega_l - \omega_r)^2 + r \dot{T}_{\mathrm{cl}}^2 \right] \mathrm{d}t \tag{59}$$

For the DM-PHEV, the combined force of engine, motor and clutch work on the system together. The cost function for this system can be described as

$$\begin{aligned} J &= \int_{t_0}^{t_f} \begin{bmatrix} q_1 (T_{\mathrm{en}} + T_{\mathrm{m1}} - T_{\mathrm{cl}})(\omega_r - \omega_l) \\ + q_2 (\omega_r - \omega_l)^2 \\ + r (\dot{T}_{\mathrm{en}} + \dot{T}_{\mathrm{m1}} - \dot{T}_{\mathrm{cl}})^2 \end{bmatrix} \mathrm{d}t \\ &\le \int_{t_0}^{t_f} \left[ x^T Q x + u^T R u \right] \mathrm{d}t \end{aligned} \tag{60}$$

where

$$Q = \begin{bmatrix} q_1 & 0 \\ 0 & q_2 \end{bmatrix}, R = r \tag{61}$$

Since the constant term C in the state-space equation is not considered, there is a steady-state error in the control. To eliminate steady-state errors, the control variable is rewritten as

$$u_{LQR} = -\begin{bmatrix} k_1 & k_2 \end{bmatrix} \begin{bmatrix} w_r - w_l \\ T_{\text{en}} + T_{\text{m1}} - T_{\text{cl}} \end{bmatrix} + T_{aux} \tag{62}$$

Equation (57) can be rewritten as

$$\dot{x} = (A - B_1 k)\, x + B_1 T_{aux} + B_2 \frac{a i_d}{R_w} \tag{63}$$

According to the final value theorem

$$\begin{aligned} x_{ss} &= \lim_{t\to\infty} x(t) = \lim_{s\to 0} sx(s) \\ &= \begin{bmatrix} -\frac{j_{le} k_2 a i_d}{k_1 R_w} + \frac{T_{aux}}{k_1} \\ \frac{j_{le} a i_d}{R_w} \end{bmatrix} \end{aligned} \tag{64}$$

To ensure that the state $x_1 = w_r - w_l$ converges to zero, additional torque demand is

$$T_{aux} = \frac{j_{le} k_2 a i_d}{R_w} \tag{65}$$

Finally, the control object in Stage 4 is transformed into the fast tracking of reference speed and the limitation of the changing rate of combined torque of motor 2 and clutch. So, in stage 4, the control object is

$$\begin{cases} x_{e3} = \omega_{\text{ref}} \\ x_{e4} = \omega_{\text{ref}} \\ J_{re}\dot{\omega}_r = T_{\text{cl}} + i_2 T_{\text{m2}} - F \\ \Delta\,(T_{\text{m1}} + T_{\text{cl}} - T_{\text{en}}) = u_{LQR} \\ \min \Delta\,(T_{\text{m2}} + T_{\text{cl}}) \end{cases} \tag{66}$$

#### *4.2.4 Control objectives in stage 5*

In this stage, clutch C2 enters engagement stage. Engine, motor 1 and motor 2 drive the DM-PHEV together, so the torque changing rate of their combined torque need to be limited.

$$j = \frac{\dot{T}_{\text{en}} + \dot{T}_{\text{m1}} + i_2 \dot{T}_{\text{m2}} - \dot{T}_f}{i_0 j_{re}} R \tag{67}$$

The torque demand of driver is transformed into the tracking of vehicle speed. So, the control object is

$$\begin{cases} x_{e3} = \omega_{\text{ref}} \\ x_{e4} = \omega_{\text{ref}} \\ (J_{re} + J_{le})\,\dot{\omega}_r = T_{\text{en}} + T_{\text{m1}} + i_2 T_{\text{m2}} - F \\ \min \Delta\,(T_{\text{m2}} + T_{\text{m1}} + T_{\text{en}}) \end{cases} \tag{68}$$

### 4.3 HC-MPC based on changing cost functions

As shown before, the cost functions change with stages. However, for H-MPC, only the state of DM-PHEV can be predicted by MLD model as the stage changes, the cost functions for the whole predictive horizon is fixed. The advantage of model prediction is to predict the future state to solve the optimal solution within a period. Fixed objectives may cause a problem that the objectives of the next several time steps changed but the controller solves the same objectives for this prediction time domain. Thus, HC-MPC is proposed in this section to acquire variable cost functions that switch with the predicted stage. Similar to the state-space equation, the cost functions are also transformed into equalities and inequalities using MLD.

The cost function of state variables changing with stages is represented as $J_{x\_\text{state}}$.

$$\begin{aligned} J_{x\_\text{state}} &= \left(Q_{1\_\text{state}}\left[x - x_{e\_\text{state}}\right]\right)\delta_{\text{state}} \\ &\Leftrightarrow \begin{cases} J_{x\_\text{state}} - M_{x\_\text{state}} \cdot \delta_i \le 0 \\ -J_{x\_\text{state}} + m_{x\_\text{state}} \cdot \delta_i \le 0 \\ J_{x\_\text{state}} - m_{x\_\text{state}} \cdot \delta_i - Q_{1\_\text{state}} \cdot x \\ \le -m_{x\_\text{state}} - Q_{1\_\text{state}} \cdot x_{e\_\text{state}} \\ -J_{x\_\text{state}} + M_{x\_\text{state}} \cdot \delta_i + Q_{1\_\text{state}} \cdot x \\ \le M_{x\_\text{state}} + Q_{1\_\text{state}} \cdot x_{e\_\text{state}} \end{cases} \end{aligned} \tag{69}$$

where, state represents different stages; $x\,(i)$ represents $i_{\text{th}}$ variable; $Q_{\text{state}}$ is weight matrix which is shown in Table 2.

Finally, the cost function of state variables can be expressed as

$$J_x = J_{x\_mot} + J_{x\_rel} + J_{x\_sli} + J_{x\_ega} \tag{70}$$

Similarly, the cost functions of $u$ and $\Delta u$ are

$$\begin{aligned} J_{u\_\text{state}} &= \left(Q_{2\_\text{state}}\left[u - u_{e\_\text{state}}\right]\right)\delta_{\text{state}} \\ &\Leftrightarrow \begin{cases} J_{u\_\text{state}} - M_{u\_\text{state}}\delta_i \le 0 \\ -J_{u\_\text{state}} + m_{u\_\text{state}}\delta_i \le 0 \\ J_{u\_\text{state}} - m_{u\_\text{state}}\delta_i + Q_{2\_\text{state}}u_{e\_\text{state}} \\ \le Q_{2\_\text{state}}\,(u_{k-1} + \Delta u_k) - m_{u\_\text{state}} + \\ -J_{u\_\text{state}} + M_{u\_\text{state}}\delta_i - Q_{2\_\text{state}}u_{e\_\text{state}} \\ \le M_{u\_\text{state}} - Q_{2\_\text{state}}\,(u_{k-1} + \Delta u_k) \end{cases} \end{aligned} \tag{71}$$

$$\begin{aligned} J_{\Delta u\_\text{state}} &= Q_{3\_\text{state}}\Delta u \delta_{\text{state}} \\ &\Leftrightarrow \begin{cases} J_{\Delta u\_\text{state}} - M_{\Delta u\_\text{state}} \cdot \delta_i \le 0 \\ -J_{\Delta u\_\text{state}} + m_{\Delta u\_\text{state}} \cdot \delta_i \le 0 \\ J_{\Delta u\_\text{state}} - m_{\Delta u\_\text{state}} \cdot \delta_i \\ \le -m_{\Delta u\_\text{state}} + Q_{3\_\text{state}} \cdot \Delta u \\ -J_{\Delta u\_\text{state}} + M_{\Delta u\_\text{state}} \cdot \delta_i \\ \le M_{\Delta u\_\text{state}} - Q_{3\_\text{state}} \cdot \Delta u \end{cases} \end{aligned} \tag{72}$$

**Table 2** Description of weight matrix

| Stage | Weight matrix |
|---|---|
| 1 | $Q_{2\_m} = \begin{bmatrix} q_2 & & & & \\ & q_2 & & & \\ & & q_2 & & \\ & & & 0 & \\ & & & & 0 \end{bmatrix}$ $Q_{3\_m} = \begin{bmatrix} q_3 & & \\ & 0 & \\ & & 0 \end{bmatrix}$ |
| 2&3 | $Q_{2\_rel} = \begin{bmatrix} 0 & & & & \\ & q_2 & & & \\ & & q_2 & & \\ & & & 0 & \\ & & & & 0 \end{bmatrix}$ $Q_{3\_rel} = \begin{bmatrix} q_3 & & \\ & 0 & \\ & & 0 \end{bmatrix}$ |
| 4 | $Q_{2\_sli} = \begin{bmatrix} 0 & & & & \\ & 0 & & & \\ & & q_2 & & \\ & & & q_2 & \\ & & & & q_2 \end{bmatrix}$ $Q_{3\_sli} = \begin{bmatrix} 0 & & \\ & q_3 & \\ & & 0 \end{bmatrix}$ |
| 5 | $Q_{2\_ega} = \begin{bmatrix} q_2 & & & & \\ & 0 & & & \\ & & q_2 & & \\ & & & 0 & \\ & & & & q_2 \end{bmatrix}$ $Q_{3\_ega} = \begin{bmatrix} 0 & & \\ & 0 & \\ & & q_3 \end{bmatrix}$ |

The equivalent cost function equalities of $u$ and $\Delta u$ are

$$\begin{cases} J_u = J_{u\_mot} + J_{u\_rel} + J_{u\_sli} + J_{u\_ega} \\ J_{\Delta u} = J_{\Delta u\_mot} + J_{\Delta u\_rel} + J_{\Delta u\_sli} + J_{\Delta u\_ega} \end{cases} \tag{73}$$

Introducing auxiliary variables

$$q = \left[ \varepsilon^x \ \varepsilon^u \ \varepsilon^{\Delta u} \right] \tag{74}$$

where

$$\begin{cases} \|J_x(i)\|_\infty \le \varepsilon^x \\ \|J_u(i)\|_\infty \le \varepsilon^u \\ \|J_{\Delta u}(i)\|_\infty \le \varepsilon^{\Delta u} \end{cases} \tag{75}$$

Finally, Eq. (75) can be translated into a MILP optimal problem as follows

$$J = \sum_{i=1}^{T} \varepsilon^{xi} + \varepsilon^{ui} + \varepsilon^{\Delta ui}$$

$$\begin{cases} x(k+1) = Ax(k) + B_1 u(k) + B_2 \delta(k) + B_3 z(k) \\ y(k) = Cx(k) + D_1 u(k) + D_2 \delta(k) + D_3 z(k) \\ E_2 \delta(k) + E_3 z(k) \le E_4 x(k) + E_1 u(k) + E_5 \\ -\varepsilon^{xi} \pm J_x(i) \le 0 \\ -\varepsilon^{ui} \pm J_u(i) \le 0 \\ -\varepsilon^{\Delta u} + J_{\Delta u}(i) \le 0 \\ T_{\mathrm{m1\_min}} \le u_1 \le T_{\mathrm{m1\_max}} \\ T_{\mathrm{m2\_min}} \le u_2 \le T_{\mathrm{m2\_max}} \\ T_{cl\_\mathrm{min}} \le u_3 \le T_{cl\_\mathrm{max}} \end{cases} \tag{76}$$

The resulting control law of HW-MPC is the same form as Eq. (49).

**Table 3** Parameters of the vehicle power-train

| Parameters | Values |
|---|---|
| Vehicle mass $m_{\mathrm{veh}}$ (kg) | 1970 |
| Front area $A$ ($\mathrm{m}^2$) | 2.66 |
| Roll resistance coefficient $f$ | 0.0116 |
| Gravity acceleration $g$ ($\mathrm{kg/m}^2$) | 9.8 |
| Air drag coefficient $C_{\mathrm{d}}$ | 0.5 |
| Final drive ratio $i_0$ | 3.8 |
| Carrier inertia $J_C$ (kg $\times\mathrm{m}^2$) | 0.0017 |
| Sun inertia $J_S$ (kg $\times\mathrm{m}^2$) | 0.0039 |
| Ring inertia $J_R$ (kg $\times\mathrm{m}^2$) | 0.0109 |
| Engine inertia $J_{\mathrm{en}}$ (kg $\times\mathrm{m}^2$) | 0.18 |
| MG1 inertia $J_{\mathrm{m1}}$ (kg $\times\mathrm{m}^2$) | 0.041 |
| MG2 inertia $J_{\mathrm{m2}}$ (kg $\times\mathrm{m}^2$) | 0.0723 |
| Wheel radius $R$ (m) | 0.353 |

## 5 Simulation and analysis

In this section, simulation and HiL test are carried out to verify the effectiveness of controller. The simulation model built in Sect. 2 is developed in MATLAB/Simulink. The main parameters of the DM-PHEV are shown in Table 3.

### 5.1 Simulation and results analysis

In the simulation, the scene of mode transition process is set as, when the vehicle speed reaches a speed of 25 km/h at 138 s, and the battery state of charge is lower than the minimum threshold, EMC gives the mode transition instruction. Then, DM-PHEV runs into mode transition process. This scenario is one case of the situation where the mode is switched and is used to verify the effectiveness of the coordinated controller.

The effects of H-MPC and HW-MPC are compared. The simulation results are given below.

States of auxiliary binary variables introduced in MLD model is shown in Fig. 11. Simulation results show that logical relations setted before is reasonable and correct. If the value of a binary variable is truth, it means that the state represented by this binary variable is worked. Binary variables shown in Fig. 11a–d are intermediate auxiliary variables introduced in event generator. The five binary variables shown in Fig. 11a represent five stages of mode transition process which

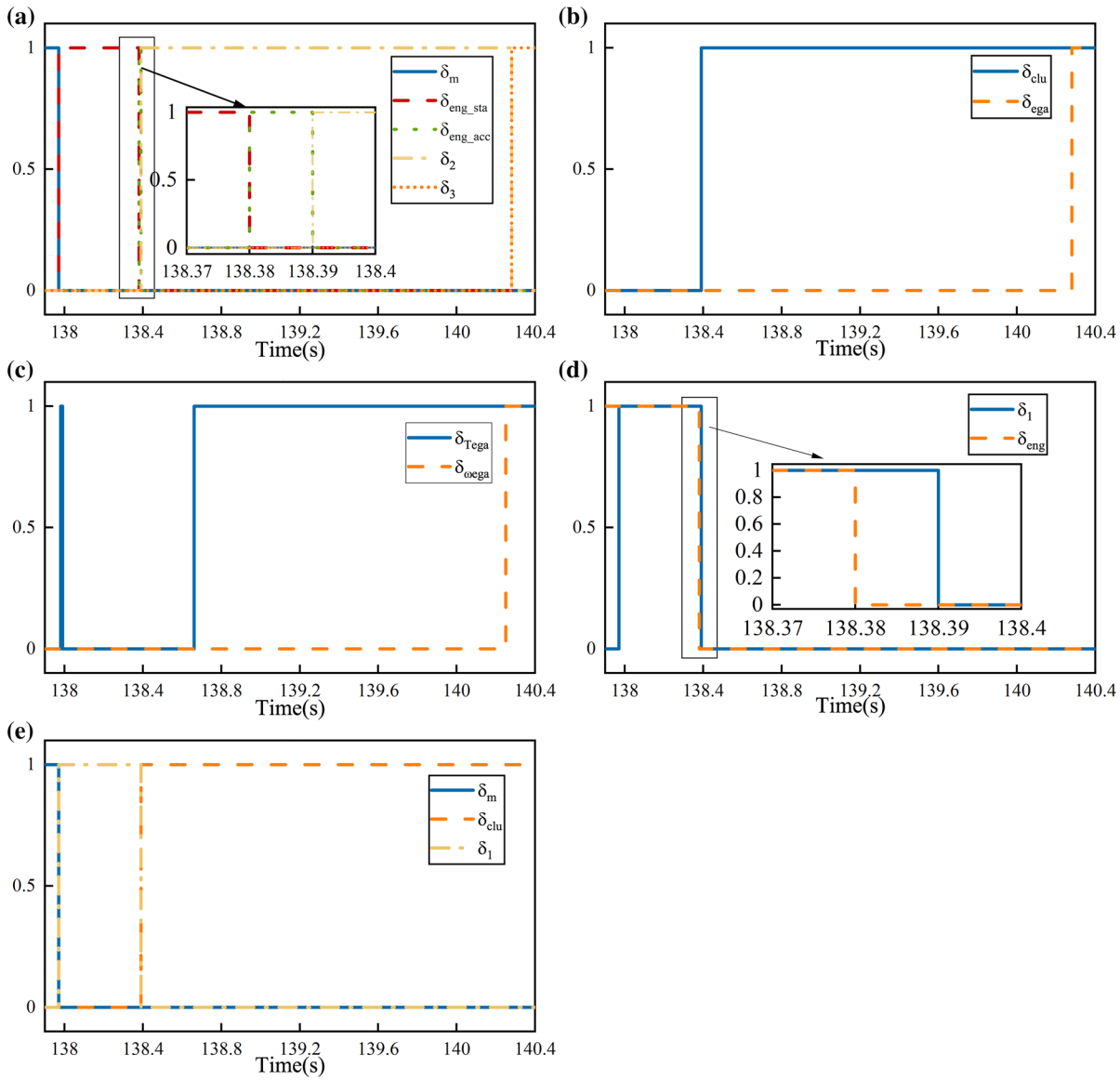


**Fig. 11** States of binary variables during mode transition process

are introduced in Mode Selector. The DM-PHEV cannot be in several stages at the same time, so only one binary variables will be truth at one time. As shown in Fig. 11a, time before 138 s is electric driving stage. Time between 138 and 138.38 s is engine start stage, and from 138.38 to 138.39 s is clutch release stage. Between 138.39 and 140.2 s is clutch slipping stage. The end is clutch engage stage.

MLD model is used by MPC controller to predict the state of DM-PHEV in the prediction time domain. In this study, the prediction horizon and control horizon are both five time steps. The results of prediction are shown in Fig. 12. From Fig. 12 it can be seen that the auxiliary binary variables which represent the stage of mode transition process can be predicted by the MLD model. The results shown in the figures are the prediction results at 138.37 s.

As shown in Fig. 12, from 138.37 s, the prediction results are: after one step, the system changes into clutch release stage from engine start stage, and then

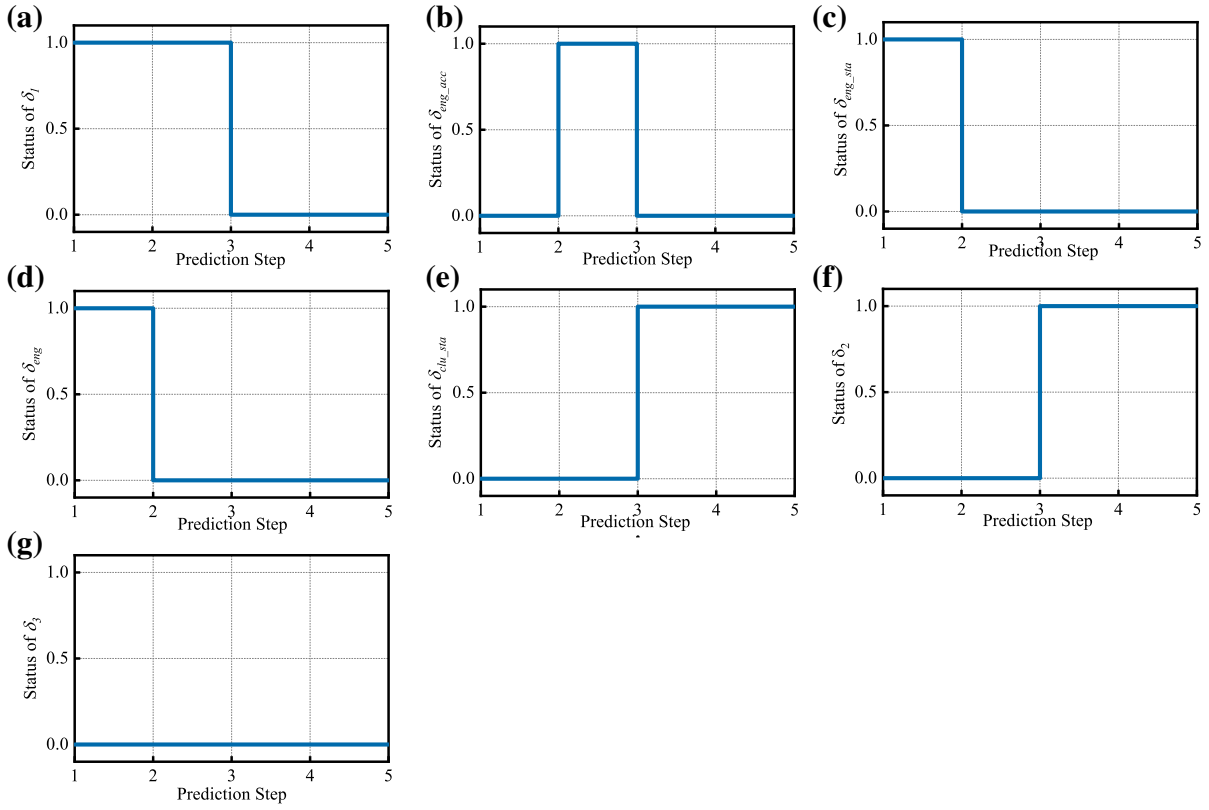


**Fig. 12** Predicted binary variables during prediction domain of HC-MPC

the third step enters clutch slipping stage and remains until the end of the predicted step.

As the coordinated controller can predict the stage of mode transition process by MLD, the states of DM-PHEV can also be predicted by controllers without discontinuity via the auxiliary continuous variables introduced in Switched Affine System. The accuracy of predicted states by MLD influence the performance of coordinated controller directly. So the comparison between the predicted state and the actual state of DM-PHEV is simulated and the results are shown in Fig. 13. The states of coordinated control system are shown in Fig. 13d–f, h. As shown in Fig. 13a–c, g, although the mathematical model of DM-PHEV changes with the stages, the auxiliary variables $z_i$ can help accurately predict the states.

Besides, HC-MPC introduced extra auxiliary variables to represent the cost functions of mode transition process which changes with stages. The simulation results of variable cost functions are shown in Figs. 14 and 15. Only the cost functions which evaluate the tracking effects on the reference speed of the two ends of clutch C2 are shown here. It can be seen that the values of cost functions shown in Figs. 14a and 15a consist of four parts which represent the corresponding evaluation index of each stage. Variable cost functions can further help the MPC to optimize the optimal solution in the predictive time domain.

The solutions of HC-MPC are the target torque of actuators as shown in Fig. 16. During the electric driving stage (time before 138 s), motor 2 drives the vehicle. Between 138 and 138.38 s, motor 1 starts the engine, so engine works as a load. At 138.38 s, engine is fired as the engine speed exceeds idle speed. To avoid the engine ripple torque, engine torque demand will keep constant during mode transition process. From 138.38 to 138.39 s, the clutch keep release and allow the motor 1 accelerate clutch driven disc to avoid the change of torque direction caused by the fluctuation of clutch speed difference. After 138.39 s, DM-PHEV enters clutch slipping stage. Clutch C2 begins to slip to decrease the speed of driven discs, which is accelerated

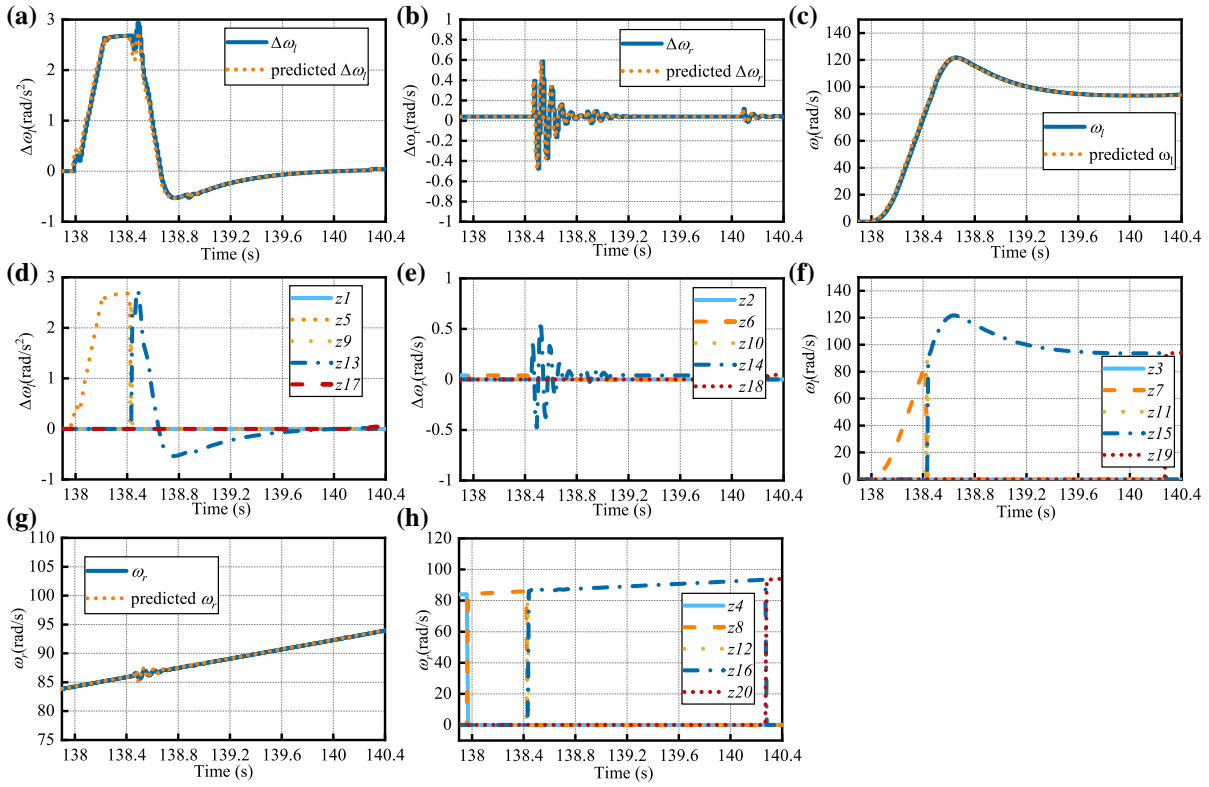


**Fig. 13** Comparison of MLD predicted value and actual state value. **a** Comparison of $\Delta\omega_l$ and predicted $\Delta\omega_l$. **b** Comparison of $\Delta\omega_r$ and predicted $\Delta\omega_r$. **c** Comparison of $\omega_l$ and $\omega_l$. **d** Value of $z_i$ representing $\Delta\omega_l$ at different stages. **e** Value of $z_i$ representing $\Delta\omega_r$ at different stages. **f** Value of $z_i$ representing $\omega_l$ at different stages. **g** Comparison of $\omega_r$ and predicted $\omega_r$. **h** Value of $z_i$ representing $\omega_r$ at different stages

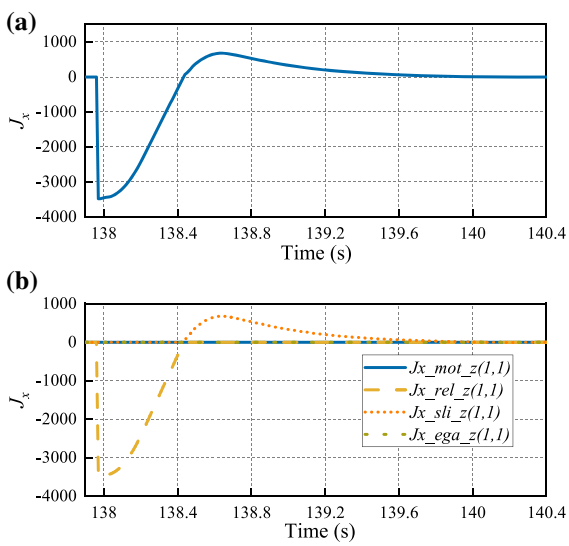


**Fig. 14** Cost functions of state variables $\omega_l$. **a** Auxiliary cost function value of $\omega_l$. **b** Auxiliary cost function values of $\omega_l$ at different stages

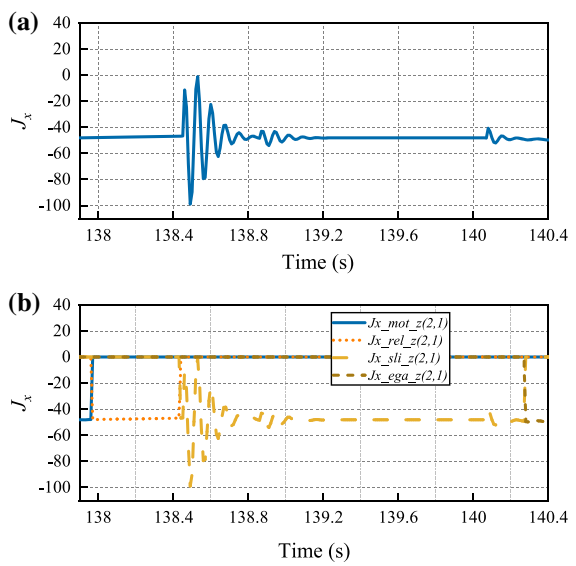


**Fig. 15** Cost functions of state variables $\omega_r$. **a** Auxiliary cost function value of $\omega_r$. **b** Auxiliary cost function values of $\omega_r$ at different stages

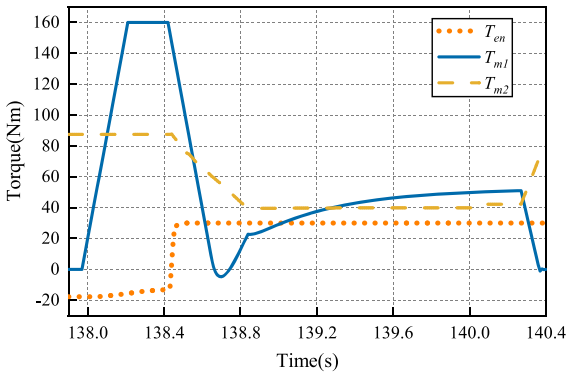


**Fig. 16** Torque command

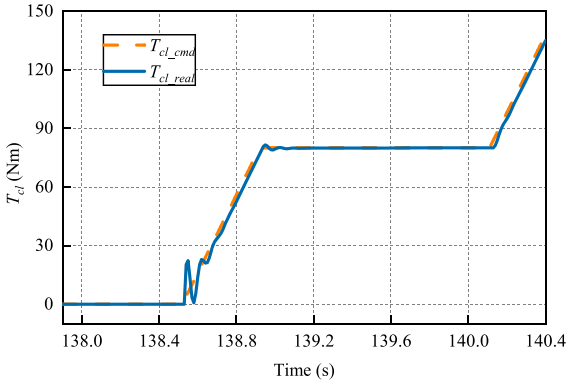


**Fig. 17** Torque of clutch

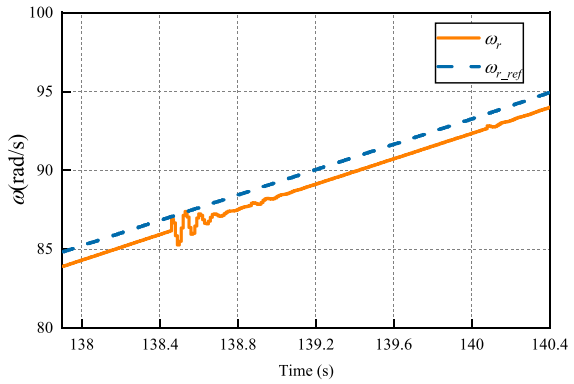


**Fig. 18** Comparison between clutch driving disc speed and reference speed

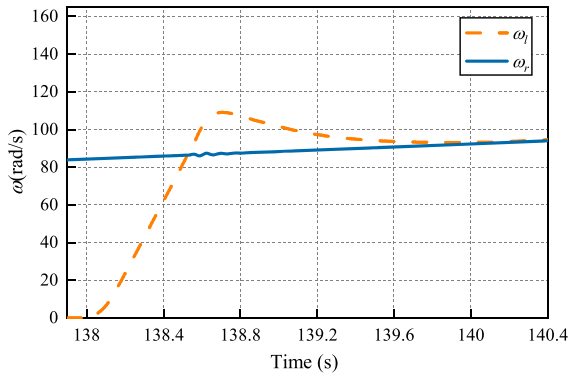


**Fig. 19** Speed comparison between clutch ends

by motor 1, so the torque of motor 1 decreases during this stage. Torque of clutch increases during this stage as shown in Fig. 17, a saturation is set on clutch torque to decrease clutch slipping energy.

The target torque is the $T_{\text{cl\_cmd}}$ in Fig. 17, the real torque transmitted by clutch $T_{\text{cl\_real}}$ is controlled by the oil pressure of its hydraulic actuator using a PID controller. As shown in Fig. 17, the tracking effect of the demand torque is relatively poor between 138.4 and 138.8 s. Because of the strong nonlinear dynamic characteristics of clutch, PID controller can hardly track the reference torque given by HC-MPC controller. The poor tracking of clutch torque results in the fluctuations of the speed of clutch driving disc as shown in Fig. 18. In addition to the fluctuations for a little time, the speed of clutch driving disc can track the reference speed smoothly. The tracking effects of clutch driven disc are shown in Fig. 19. It can be seen that clutch engagement process is smooth to reduce vehicle jerk. The comparison of speed difference between clutch ends of HC-MPC and H-MPC is shown in Fig. 20. The speed difference controlled by HC-MPC is faster and more smooth close to zero. The torque shown in Fig. 21 is equal to $T_{\text{cl}} - (T_{\text{en}} + T_{\text{m1}})$. In the clutch slipping stage, the torque transmitted by clutch is $T_{\text{cl}}$, and when the mode transition process enters into clutch engagement stage, the torque transmitted by clutch is $T_{\text{en}} + T_{\text{m1}}$, to reduce the vehicle jerk at the moment of clutch engagement, the torque $T_{\text{cl}} - (T_{\text{en}} + T_{\text{m1}})$ should be close to zero at the end of clutch slipping stage as shown in Fig. 21.

The duration for each stage of mode transition process shown in these figures are consistent with the results in Fig. 11.

As described in Sect. 3, the performance of HC-MPC can be characterized by three objectives which is shown in Figs. 22, 23 and 24, respectively. From Fig. 22, it can be seen that the power demand of driver can be satisfied, and the speed keeps smoothly.

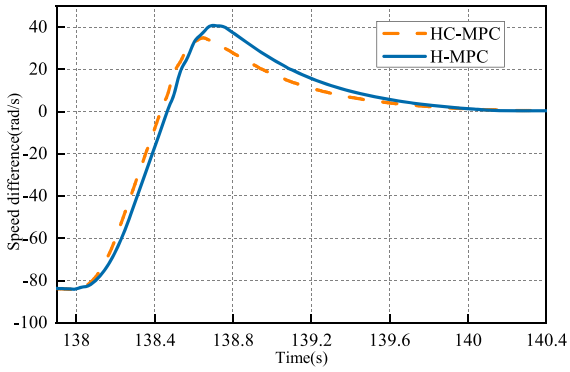


**Fig. 20** Comparison of speed difference between clutch ends

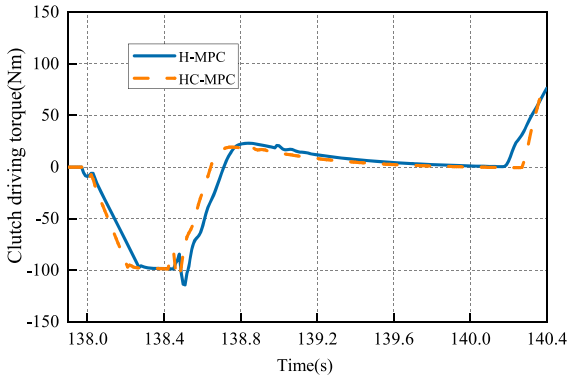


**Fig. 21** Force on clutch driven disc

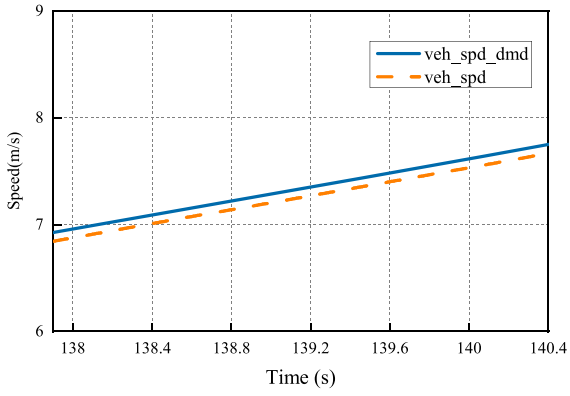


**Fig. 22** Vehicle speed

The changing trend of jerk is consistent with the speed of clutch driving disc shown in Fig. 18. The fluctuation of clutch torque from 138.5 to 139 s shown in Fig. 17 revealed the source of vehicle jerk. As shown in Fig. 23, the simulated vehicle jerk intensity controlled by HC-MPC can be controlled to within 10 m/s$^3$, which is similar to the performance of H-MPC. At 140 s,

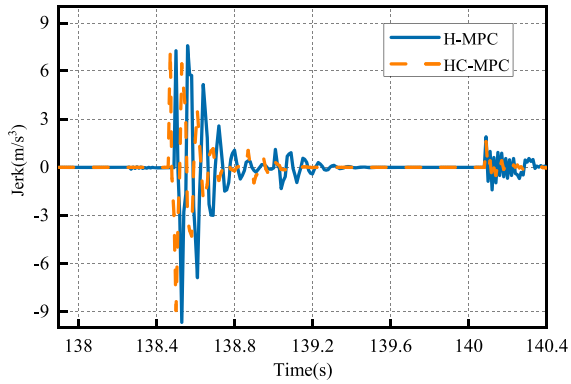


**Fig. 23** Vehicle jerk

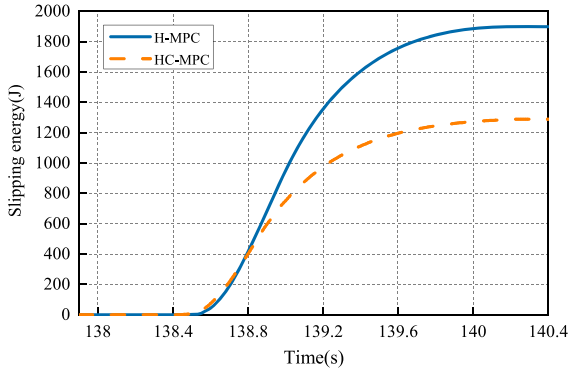


**Fig. 24** Slipping energy loss

the maximum jerk of HC-MPC is about 9% smaller than that of H-MPC, as the object of HC-MPC is more clear than that of H-MPC, which helps it early predict engagement stage and reduced the acceleration of the clutch driven disc to avoid jerk. From Fig. 21 it can be seen that the torque of Motor determined by HC-MPC changes frequently to suppress the jerk of vehicle from 138.5 to 139 s.

The vehicle jerk after 140s is caused by the clutch engagement process, as the torque $T_{\mathrm{cl}} - (T_{\mathrm{en}} + T_{\mathrm{m1}})$ is not completely equal to zero.

The clutch slipping energy loss is shown in Fig. 24. Clutch controlled by HC-MPC consumed about 1200 J, while clutch controlled by H-MPC consumed 1800 J, the former is about 50% better than the latter. From Fig. 20 we can conclude that HC-MPC can engage the clutch C2 quicker than H-MPC and the speed difference controlled by HC-MPC is smaller than that controlled by H-MPC, so the energy slipping loss of HC-MPC is lower than that of HC-MPC. Thus, HC-MPC can obtain

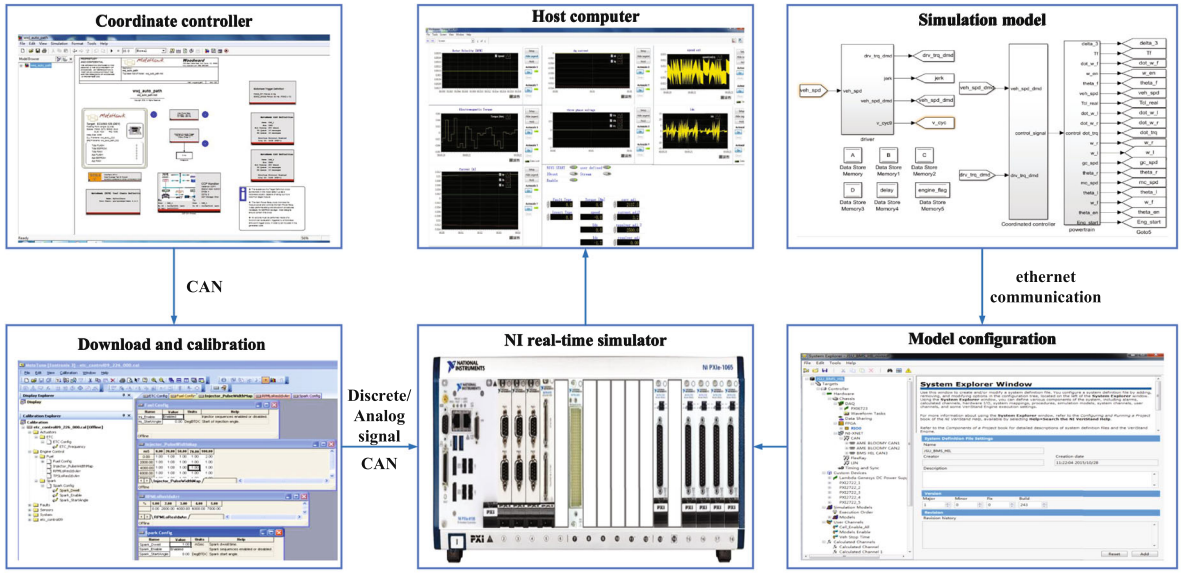


**Fig. 25** Schematic diagram of HiL test

smaller clutch slipping energy while cause similar vehicle jerk H-MPC, which helps minimize the clutch discs abrasion and prolong the life of clutch.

### 5.2 HiL test and results analysis

A HiL test is carried out to verify the real-time effect of the HW-MPC. The schematic diagram of HiL test is shown in Fig. 25. The HiL experiment environment consists of NI real-time simulator, Chroma programmable power supply, Bloomy battery simulator and rapid prototype controller. The coordinated control strategy is designed by MATLAB/Simulink, then the strategy will be compiled and downloaded into the real controller. The DM-PHEV model is also built in MATLAB/Simulink, which is downloaded into NI real-time simulator to simulate the operation of PHEV. The control signals of controller are transmitted to NI by controller area network (CAN) bus [33]. The HiL test condition is the same as the simulation condition as shown before.

The test results are shown in Fig. 26, which are similar to the simulation results. As shown in Fig. 26a, at about 137.8 s, motor 1 begins to start the engine, then engine ignites at about 138.8 s. During clutch slipping stage, it can be seen from Fig. 26c that speed of driven disc of clutch reaches to the speed of driving disc smoothly as expected by means of coordinated control between engine, motor 1, motor 2 and clutch C2. Figure 26f is the comparison between speed of driving disc and reference speed, which suggests that the coordinate controller can meet driver torque demand. Riding comfort is measured by vehicle jerk in Fig. 26g. The communication delay caused by CAN bus can be regarded as disturbances. These disturbances excited unexpected vehicle jerks, so both the effects of H-MPC and HC-MPC are worse than simulation, but the results are within the criterion, and effects of HC-MPC are better than H-MPC. Due to the speed difference of the two ends of clutch are bigger than results of simulation as shown in Fig. 26d, the clutch slipping energy consuming is also more than results of simulation. But the energy consumed by HC-MPC is still less than that consumed by H-MPC. The quantitative results are shown in Table 4. In short, the HiL test results verified the effectiveness of the proposed HC-MPC coordinate control strategy.

## 6 Conclusion

This paper discusses the mode transition process from EM to HM of a DM-PHEV. The main conclusions show the following:

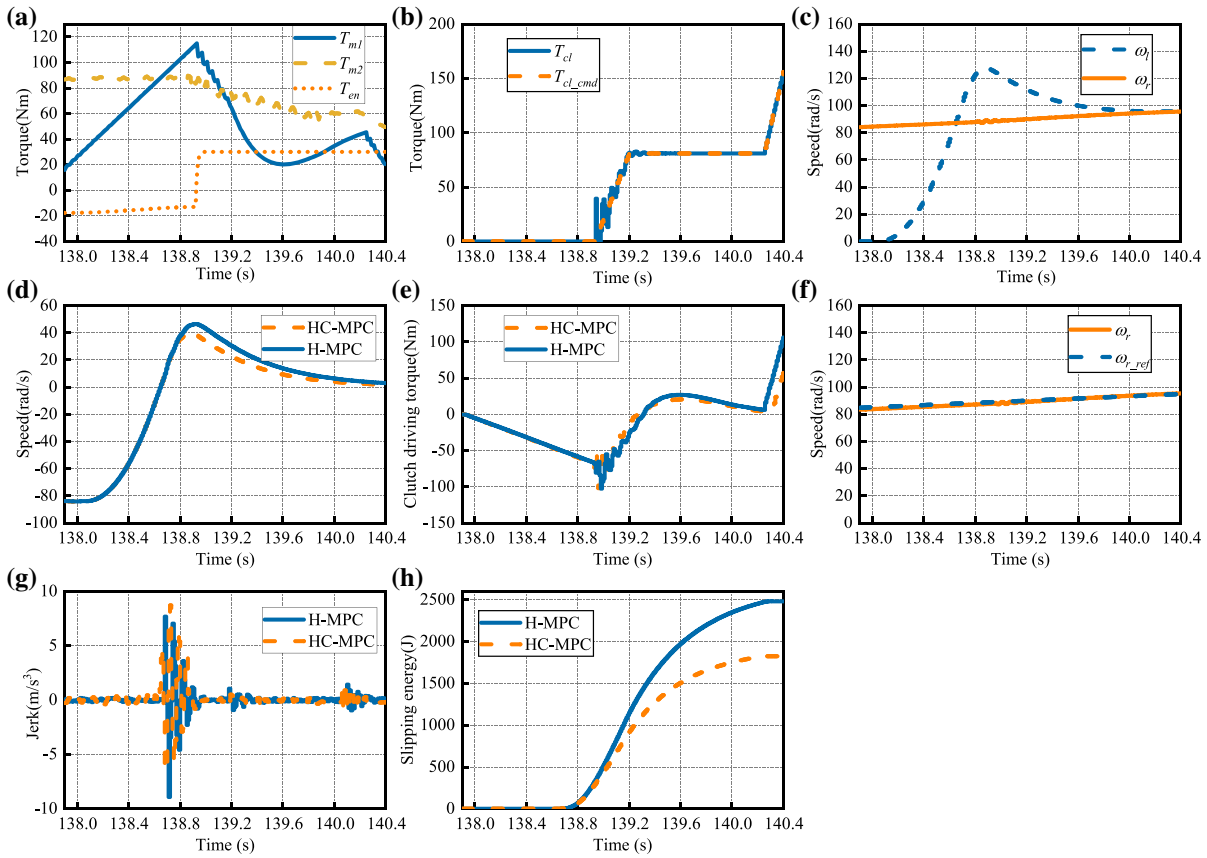


**Fig. 26** HiL results. **a** Torque command. **b** Comparison of torque command of clutch and actual clutch torque. **c** Comparison of speed of driven and driving discs of clutch. **d** Comparison of speed difference of HC-MPC and H-MPC. **e** Comparison of clutch driving force of HC-MPC and H-MPC. **f** Comparison of actual $\omega_r$ and reference $\omega_{r\_ref}$. **g** Comparison of jerk. **h** Comparison of slipping energy

**Table 4** Quantitative comparison results of HiL

| | HC-MPC | H-MPC | Improvement (%) |
|---|---|---|---|
| Jerk (m/s$^3$) | 8.7 | 8.9 | 2.3 |
| Energy loss (J) | 1824 | 2480 | 35.9 |

1. A plant model of DM-PHEV is developed that considered the dynamic characteristics of engine, motors, clutch and power-train. This model can be used to simulate the actions of DM-PHEV during mode transition process, which can help verify the coordinated control strategy.
2. The mode transition process of DM-PHEV is analysed and hybrid dynamic model of it is built. According to the status of engine and clutch, the mode transition process is divided into five stages. To achieve a smooth mode transition process, lower energy consumption and quick engine start, hybrid dynamic model is built by MLD which considers the different characteristics of each stages.
3. Control objectives are proposed and a H-MPC controller is designed. Furthermore, the cost function should change with the mode transition stage, so a HC-MPC is proposed so that the cost function can changed in the predictive process of MPC.

4. Simulations and HiL tests are carried out to verify the proposed control strategy. The simulation results show that the proposed HC-MPC controller can achieve the object of mode transition: The vehicle jerk is within acceptable range and the clutch energy loss is reduced by about 50% than that of H-MPC. HiL test also suggests the effectiveness of the strategy.

In short, the proposed control strategy can improve the mode transition performance of the DM-PHEV, and can provide a theoretical reference for the PHEV in engineering practice. In the future, considering that the jerk is mainly caused by the torque error of clutch, so a controller aiming at the nonlinear dynamics of wet clutch actuating system should be studied for mode transition process to improve the ride comfort of DM-PHEV.

**Acknowledgements** This work is financially supported by the National Key Research and Development Project [No. 2017YFB0103200], the National Natural Science Foundation of China [No. 51705204], Six Talent Peaks Project in Jiangsu Province (CN) [No. JXQC-036], the China Scholarship Council [No. 201908320221].

**Compliance with ethical standards**

**Conflicts of interest** The authors declare that they have no conflict of interest.

## References

1. Malikopoulos, A.A.: Supervisory power management control algorithms for hybrid electric vehicles: a survey. IEEE Trans. Intell. Transport. Syst. **15**(5), 1869–1885 (2014)
2. Zhang, F., Hu, X., Langari, R., Cao, D.: Energy management strategies of connected hevs and phevs: recent progress and outlook. Prog. Energy Combust. Sci. **73**, 235–256 (2019)
3. Wang, F., Zhang, J., Xu, X., Cai, Y., Zhou, Z., Sun, X.: New teeth surface and back (TSB) modification method for transient torsional vibration suppression of planetary gear powertrain for an electric vehicle. Mech. Mach. Theory **140**, 520–537 (2019)
4. Wang, F., Zhang, J., Xu, X., Cai, Y., Zhou, Z., Sun, X.: New method for power allocation of multi-power sources considering speed-up transient vibration of planetary power-split hevs driveline system. Mech. Syst. Signal Process. **128**, 1–18 (2019)
5. Hung, Y.H., Tung, Y.M., Chang, C.H.: Optimal control of integrated energy management/mode switch timing in a three-power-source hybrid powertrain. Appl. Energy **173**, 184–196 (2016)
6. Martinez, C.M., Hu, X., Cao, D., Velenis, E., Gao, B., Wellers, M.: Energy management in plug-in hybrid electric vehicles: recent progress and a connected vehicles perspective. IEEE Trans. Veh. Technol. **66**(6), 4534–4549 (2017)
7. Zeng, X., Wang, J.: Optimizing the energy management strategy for plug-in hybrid electric vehicles with multiple frequent routes. IEEE Trans. Control Syst. Technol. **27**(1), 394–400 (2019)
8. Liu, J., Chen, Y., Li, W., Shang, F., Zhan, J.: Hybrid-trip-model-based energy management of a phev with computation-optimized dynamic programming. IEEE Trans. Veh. Technol. **67**(1), 338–353 (2018)
9. Wang, F., Zhang, J., Xu, X., Cai, Y., Zhou, Z., Sun, X.: A comprehensive dynamic efficiency-enhanced energy management strategy for plug-in hybrid electric vehicles. Appl. Energy **247**, 657–669 (2019)
10. Xu, X., Zhang, T., Wang, F., Wang, S., Zhou, Z.: Integrated energy management strategy of powertrain and cooling system for phev. Int. J. Green Energy **17**(5), 319–331 (2020)
11. Wang, C., Zhao, Z., Zhang, T., Li, M.: Mode transition coordinated control for a compound power-split hybrid car. Mech. Syst. Signal Process. **87**, 192–205 (2017)
12. Zeng, X., Yang, N., Wang, J., Song, D., Zhang, N., Shang, M., Liu, J.: Predictive-model-based dynamic coordination control strategy for power-split hybrid electric bus. Mech. Syst. Signal Process. **60–61**, 785–798 (2015)
13. Liu, W.: Introduction to hybrid vehicle system modeling and control, pp. 299–323 (2013)
14. Shen, D., Guehmann, C., Zhang, T.: Coordinated mode transition control for a novel compound power-split hybrid electric vehicle. In: WCX SAE World Congress Experience (2019)
15. Yang, C., Shi, Y., Li, L., Wang, X.: Efficient mode transition control for parallel hybrid electric vehicle with adaptive dual-loop control framework. IEEE Trans. Veh. Technol. **69**(2), 1519–1532 (2020)
16. Yang, C., Jiao, X., Li, L., Zhang, Y., Chen, Z.: A robust h-infinity control-based hierarchical mode transition control system for plug-in hybrid electric vehicle. Mech. Syst. Signal Process. **99**, 326–344 (2018)
17. Wang, F., Xia, J., Xu, X., Cai, Y., Zhou, Z., Sun, X.: New clutch oil-pressure establishing method design of phevs during mode transition process for transient torsional vibration suppression of planetary power-split system. Mech. Mach. Theory **148**, 103801 (2020)
18. Song, S., Guan, Y., Fu, Z., Li, H.: Switching control from motor driving mode to hybrid driving mode for phev. In: 2017 Chinese Automation Congress (CAC), pp. 4209–4214 (2017)
19. Gao, A., Fu, Z., Tao, F.: Dynamic coordinated control based on sliding mode controller during mode switching with ice starting for an hev. IEEE Access **8**, 60428–60443 (2020)
20. Branicky, M.S., Borkar, V.S., Mitter, S.K.: A unified framework for hybrid control: model and optimal control theory. IEEE Trans. Autom. Control **43**(1), 31–45 (1998)
21. Bemporad, A., Heemels, W.P.M.H., De Schutter, B.: On hybrid systems and closed-loop mpc systems. IEEE Trans. Autom. Control **47**(5), 863–869 (2002)
22. Bemporad, A., Morari, M.: Control of systems integrating logic, dynamics, and constraints. In: Automatica, vol. 35 (1999)
23. Kou, Z., Song, C., Pan, Z.: Mld-based predictive control of energy management for hybrid electric bus. In: Proceed-

ings of the 10th World Congress on Intelligent Control and Automation, pp. 2806–2811 (2012)
24. Sun, X., Zhang, H., Cai, Y., Wang, S., Chen, L.: Hybrid modeling and predictive control of intelligent vehicle longitudinal velocity considering nonlinear tire dynamics. Nonlinear Dyn. **97**, 1–16 (2019)
25. Su, Y., Hu, M., Su, L., Qin, D., Zhang, T., Fu, C.: Dynamic coordinated control during mode transition process for a compound power-split hybrid electric vehicle. Mech. Syst. Signal Process. **107**, 221–240 (2018)
26. Zhao, C., Zu, B., Xu, Y., Wang, Z., Zhou, J., Liu, L.: Design and analysis of an engine-start control strategy for a single-shaft parallel hybrid electric vehicle. Energy **202**, 117621 (2020)
27. Hongwei, H., Hequan, W., Zhiyong, Z., Yimin, S.: Research on trajectory tracking control for wet clutch engagement based on smc. Procedia Eng. **15**, 2742–2746 (2011)
28. Zhang, H., Qin, Y., Li, X., Liu, X., Yan, J.: Power management optimization in plug-in hybrid electric vehicles subject to uncertain driving cycles. eTransportation **3**, 100029 (2020)
29. Bemporad, A., Morari, M.: Predictive control of constrained hybrid systems. In: Nonlinear Model Predictive Control, pp. 71–98 (2000)
30. Bemporad, A., Borrelli, F., Morari, M.: Piecewise linear optimal controllers for hybrid systems. In: Proceedings of the 2000 American Control Conference. ACC (IEEE Cat. No. 00CH36334), vol. 2, pp. 1190–1194 (2000)
31. Borrelli, F., Bemporad, A., Fodor, M., Hrovat, D.: An mpc/hybrid system approach to traction control. IEEE Trans. Control Syst. Technol. **14**(3), 541–552 (2006)
32. Zhou, S., Walker, P., Tian, Y., Zhang, N.: Mode switching analysis and control for a parallel hydraulic hybrid vehicle. Veh. Syst. Dyn. 1–21 (2020)
33. Zhang, H., Zhang, Y., Yin, C.: Hardware-in-the-loop simulation of robust mode transition control for a series-parallel hybrid electric vehicle. IEEE Trans. Veh. Technol. **65**(3), 1059–1069 (2016)